REVIEW ARTICLE OPEN

Check for updates

Alteration of medieval stained glass windows in atmospheric medium: review and simplified alteration model

Aurélie Verney-Carron[1] ✉, Loryelle Sessegolo[1], Anne Chabas[1], Tiziana Lombardo[2], Stéphanie Rossano[3], Anne Perez[3], Valentina Valbi[3], Chloé Boutillez[3], Camille Muller[3], Cyril Vaulot[4,5], Barbara Trichereau[6,7] and Claudine Loisel[6,7]

Stained glass windows are a precious heritage to pass on to future generations. However, medieval stained glass windows are particularly altered due to their chemical composition and the effects of climatic (mainly water and temperature), environmental (pollution) and biological factors. In this review, we present the alteration patterns observed on ancient Si-K-Ca stained glass windows. To better understand their formation mechanisms and determine the alteration rates, different exposure campaigns to the current atmosphere in a position sheltered from rain or not and laboratory experiments in aqueous medium or in gaseous phase have been conducted. Either model glass or ancient stained glass windows were studied. Isotopic tracers (D, ^{18}O, ^{29}Si) have been used as they constitute a powerful tool to elucidate the involved processes and to measure their kinetics. Thanks to all of these data, an alteration scenario of medieval stained glass alteration is proposed. Besides, the extrapolation of kinetic data based on several hypotheses over seven centuries gives very consistent results compared to the ancient stained glass samples.

npj Materials Degradation (2023)7:49 ; https://doi.org/10.1038/s41529-023-00367-0

INTRODUCTION

The majority of stained glass windows were produced during the Middle Ages as ornament of religious buildings, especially in Europe. Archeological excavations attest to the first evidence of glass pieces held together by leads as early as the fourth–fifth centuries. However, the stained glass really develops in the twelfth century thanks to the orders of daring ecclesiastics and then in the thirteenth century when its installation becomes generalized.

The stained glass windows transmit the light through glass pieces that can be transparent or translucent, raw, colored in the mass through the addition of chromophore elements such as Cu, Fe, Mn, Co, etc.[1–6], flashed (red glass) or decorated on the surface (with grisaille, yellow stain, enamels, engravings or cold paint). Grisaille, an opaque glass paint, was widely used in the thirteenth century too. It consists of a colorant (usually Cu and/or Fe oxides), a flux (usually leaded glass) and a binder (e.g. vinegar, gum arabic). In France, yellow stain, obtained with silver salt mixed with a binder, appeared at the beginning of the fourteenth century[7]. Many glass pieces (between 2 and 4 mm thick) are mounted side by side and are held together by a lead came, constituting a panel. The panel is then fixed and strengthened by an ironwork (saddle-bars sealed in the masonry, lug bars, cover plates, wedges)[8].

This heritage has survived the centuries, exposed to the atmosphere, weathering agents, microorganisms and anthropic activity (pollution and degradation). Many factors can influence the alteration, such as rain quantity, composition and pH, temperature, wind, relative humidity, gas concentration (SO_2, NO_2, O_3, CO_2, etc.) and particulate matter in the atmosphere or different microorganisms (bacteria, lichens, algae, fungi, etc.). The combination of these altering factors and the low durability of these glasses (induced by their composition) cause significant modifications of physical and chemical properties on their surface. This leads to the formation of an altered layer and of secondary products. A great diversity of alteration patterns and intensities can be observed. This can be explained both by variable glass chemical compositions and by the environmental parameters that are constantly changing, both outdoors and indoors (e.g. Camuffo et al.[9]), in time and in space. The progression of the alteration modifies, among other things, the optical and esthetic properties of the material.

The techniques and ethics of restoring these pieces have evolved over time toward more and more caution and respect, with gentle methods and constant monitoring of the actions taken. At the same time, conserving the windows requires regular monitoring and overall cleaning interventions aimed at maintaining the glass on a condition judged suitable: removal of deposits and dust with chemical (solvent applied with poultice or gel) or mechanical (soft brush, scalpel, glass fiber) methods; biocide treatments before intervention)[8]. More recently, cleaning protocols with femto-second pulsed lasers showed relevant results[10]. Another current technique developed for prevention and conservation is the installation of protective glazing[11–13].

Nevertheless, the deterioration of stained glass occurs. The knowledge of the physical, chemical and biological mechanisms of alteration according to the different environmental parameters, independent and coupled, as well as the associated kinetics, are key to anticipate their alteration. Besides, glass alteration understanding is an issue whose scope goes beyond that of heritage and the conservation of works of art such as stained glass windows. Developing predictive models is also important in the case of nuclear glasses used to store moderately and highly radioactive waste as they have to be durable for thousands of years[14,15] and in the case of basaltic glass and their implications on biogeochemical cycles (e.g. Prause et al.[16]).

[1]Université Paris Est Creteil and Université Paris Cité, CNRS, LISA, F-94010 Créteil, France. [2]Swiss National Museum, Collection Centre, CH-8910 Affoltern am Albis, Switzerland. [3]Laboratoire Géomatériaux et Environnement, Université Gustave Eiffel, F-77454 Marne-la-Vallée, France. [4]Université de Haute-Alsace, Institut de Science des Matériaux de Mulhouse (IS2M), CNRS UMR 7361, F-68100 Mulhouse, France. [5]Université de Strasbourg, F-67081 Strasbourg, France. [6]Laboratoire de Recherche des Monuments Historiques, Centre de Recherche sur la Conservation (CRC), Muséum National d'Histoire Naturelle, CNRS, Ministère de la Culture, F-77420 Champs-sur-Marne, France. [7]Centre de Recherche sur la Conservation, F-75005 Paris, France. ✉email: aurelie.verney@lisa.ipsl.fr

In order to better preserve and restore stained glass windows, that are a precious heritage to pass on to future generations, it is therefore important to know the morphology of the alterations, to understand the mechanisms involved and to determine the kinetics of these mechanisms as a function of glass composition and environment. The objective is to develop models that are able to account for the alteration history and to predict the alteration in the future (in the context of the climate change or the evolution of pollution). This is the purpose of this review. Thus, in this paper, we first present the range of chemical composition of medieval stained glass windows studied for their alteration, then we describe the general phenomenology of stained glass alteration, the involved mechanisms and the main factors that control the kinetics. Thanks to this synthesis of previous works, their alteration history through centuries was reconstructed.

THE MEDIEVAL GLASS COMPOSITION

The medieval stained glass composition is highly variable as it has evolved through time[17–22], it depends from the geographical zone and from the raw materials[23]. Medieval glasses are most often K-rich due to their recipe, except for some Na-rich glass produced with different raw materials or ancient glass (e.g., Chartres blue[24]). At that time, glass was elaborated in forests where the glass-makers found sand, wood, plants whose calcination brings the main modifier elements (K, Ca) and minerals rich in metallic oxides for the coloring. Thereafter, the stained glasses adopt mostly a sodic composition. Adlington et al.[23] have compiled 1329 analyses of major elements in glass dating from the twelfth to the fifteenth centuries to discriminate three regional composition types (northwestern France, around Rhine and Central Europa). They are particularly distinguished by their content in Mg (inversely correlated to Ca) and in P.

Table 1 lists the composition of Si-K-Ca stained glass windows whose alteration was reported in the literature. The SiO_2 content varies between 40 and 62 wt% (50 ± 5 wt% in average). The content of other oxides is: between 0.6 and 4.2 wt% for Al_2O_3 (1.8 ± 0.7 wt% on average), 4.6 and 26.1 wt% for K_2O (17.6 ± 4.6 wt% on average), 10.4 and 29.2 wt% for CaO (17.8 ± 4.0 wt% on average), 1.5 and 10.4 wt% for MgO (4.5 ± 1.6 wt% on average), 0.1 and 4.6 wt% for Na_2O (1.0 ± 0.9 wt% on average). The concentrations in MnO, P_2O_5, FeO or Fe_2O_3, TiO_2 are also variable. Manganese, when MnO is higher than 1–2 wt%, is assumed to be intentionally added as a coloring (or decoloring) agent[2,21,25–27], whereas phosphorus is mainly provided by ashes, iron by plant ashes and titanium by sand[21,28]. The concentration of elements (e.g. cobalt or copper) used for the coloration of glass is obviously dependent of the glass piece.

However, because of the poor silica content and the high content in modifiers, these Si-K-Ca glasses are low durable and highly sensitive to weathering[29–31].

ALTERATION PHENOMENOLOGY OF ANCIENT STAINED GLASS WINDOWS

In this section, we will focus only on the alteration of glass itself. The degradation of grisaille is specific[32,33] and is out of the scope of this review.

Alteration layer morphology

Stained glass windows on monuments can sometimes appear blackened, opaque and tarnished (Fig. 1). Indeed, atmospheric conditions cause the development of an alteration layer whose morphology and composition differ as a function of alteration conditions.

Many studies have characterized the altered layers of stained glass windows dating back to the Middle-Ages (see Table 2). The altered layer is generally amorphous, rich in Si, Al and Fe and depleted in Ca, Mg, Na and K. Local enrichments in Pb, Mn and Zn are often detected.

The morphology is very heterogeneous. Different states of alteration are observed: no or little alteration (with a slight dealkalization), isolated pits of variable size that lead to craters (Fig. 1a, c, e) or a continuous alteration layer with perpendicular cracks that can penetrate deep into the pristine glass and create some digitations (Fig. 1b, d, f). The glass surface can also be colonized by microorganisms (Fig. 1h). Beyond the specific patterns that they can induce, they can be visible in the case of lichens, algae, etc. or if they form biofilms of significant thickness (up to 150 µm)[34,35]. The differences in alteration stages (from isolated pits to their coalescence, which forms a uniform layer) can be explained by the alteration time, the environmental conditions (more or less sheltered exposure, climate, pollution) and glass chemical composition. In general, discontinuous pits are rather observed indoor or outdoor in sheltered position from rain. Craters and continuous altered layers are observed in outdoor environment. These differences seem to confirm that these patterns are due to different conditions of water exposure.

In the case of pits, the alteration progresses in a radial way while in the case of a continuous layer, the front advances parallel to the initial surface. A study of Sessegolo et al.[36] focused on the impact of initial surface defects on the medieval-type glass alteration (in aqueous medium). The authors have altered medieval-type model glass (SG3, see composition in Table 3) coupons with three different roughness levels (polished at different initial grades) for 6 months in pure water at 30 °C. The initial surface defects have a high impact on the alteration morphology. For smooth samples (initially polished down to the quarter of micron), the altered layer has a constant thickness with an alteration front parallel to the initial surface. The alteration layer is composed of different sub-layers that can peel-off over time (similarly to what was observed by Gentaz et al.[37]). On the contrary, rougher samples have a heterogeneous altered layer. Defect surfaces are amplified by the alteration that favors local saturation and phase precipitation inside them. The initial defects can therefore influence the alteration layer morphology.

Several authors have also observed laminations within the altered layers of stained glass[38,39], as in the case of ancient immersed glasses[40–42], buried archeological glasses[24,43–55], basaltic glasses[56], and nuclear glasses under certain conditions[57].

In addition, the cycles of humidification/drying cause the appearance of mechanical stresses in the layer leading to its cracking, or even loss of material over time. The cracks and loss of material can give direct access to water to the pristine glass which is no longer protected[37]. It is also commonly observed that secondary phases precipitate within the crack network of the alteration layer[37]. These phases induce strong mechanical stresses as they can be hygroscopic (absorption of water that changes their properties) or deliquescent (if they become liquid). Thus their state change with variations in relative humidity or in case of rain. They can also be a cause of loss of material from the altered layer over time.

Alteration thickness

Table 2 shows that the altered thickness of stained glass windows dating from the Middle Ages (thirteenth–fourteenth centuries) can vary from values close to 0 (when alteration is in the form of pits with almost pristine areas between them) until about 300 µm in atmospheric medium (and even 1 to 3 mm in extreme cases). Some buried glass samples also display a layer up to a millimeter thick[24]. The apparent alteration rate (corresponding to the measured alteration thickness divided by the sample age) varies between 0.08 and 1.6 µm $year^{-1}$ for stained glasses buried in soils

Table 1. Chemical composition (in wt%) of Si-K-Ca stained glass windows from different sites (local names) sorted by country.

Ref	Site	Name/nb of samples	Color	Date	SiO_2	Al_2O_3	K_2O	CaO	MgO	MnO	Na_2O	Fe_2O_3/FeO*	P_2O_5	TiO_2	CuO/Cu_2O*/Cu**	PbO/Pb*	SO_2/SO_3*	Cl^-	Others	Tot.
	Portugal																			
33	Mosteiro da Batalha	group I	n.d.	XV–XVI	60.22	n.d.	17.76	12.23	n.d.	1.63	n.d.	0.76	n.d.	0.16	6.09	0.14	n.d.	n.d.	0.50	99.0
	Spain																			
163	Catedral de Tarragona	T-22	blue	XIV–XV	43.22	2.15	17.13	17.83	4.65	1.13	0.34	0.99*	3.62	0.14	0.17	0.08	n.d.	n.d.	0.02	90.5
163		T-2	blue	XIV–XV	45.77	2.26	15.49	18.12	4.78	1.13	0.33	0.99*	3.39	0.16	0.21	0.06	n.d.	n.d.	0.03	91.7
163		T-41	blue	XIV–XV	41.99	2.21	17.74	18.21	4.86	0.00	0.37	0*	3.47	0.15	0.19	0.08	n.d.	n.d.	0.01	89.3
163		T-32	br.-ye.	XIV–XV	47.91	2.18	18.95	17.32	4.68	1.00	0.33	0.45*	3.53	0.15	0.06	0.03	n.d.	n.d.	0.01	96.1
163		T-5	noc.	XIV–XV	48.17	2.22	18.26	17.92	4.79	1.04	0.38	0.46*	3.82	0.15	0.09	0.06	n.d.	n.d.	0.01	96.9
163		T-40	pu.	XIV–XV	40.19	0.65	15.59	22.41	4.42	0.64	0.38	0.26*	1.24	0.10	0.00	0.04	n.d.	n.d.	0.01	85.7
163		T-6	red-f.	XIV–XV	46.27	2.32	17.90	17.99	4.83	1.03	0.37	0.44*	3.79	0.14	0.40	0.06	n.d.	n.d.	0.02	95.1
163		T-31	red-f.	XIV–XV	48.61	2.27	18.84	17.54	4.69	1.00	0.36	0.52*	4.33	0.17	0.32	0.01	n.d.	n.d.	0.01	98.1
163		T-35	red-f.	XIV–XV	41.53	2.30	17.15	17.15	4.49	1.07	0.41	0.47*	3.45	0.16	0.39	0.08	n.d.	n.d.	0.03	88.2
164		T-1	blue	XIV	47.11	2.34	18.47	18.64	4.87	1.22	0.33	1.05*	3.93	0.15	0.21	0.15	n.d.	n.d.		97.4
164		T-2	noc.	XIV	48.17	2.23	18.26	17.92	4.79	1.04	0.38	0.46*	3.82	0.11	0.09	0.06	n.d.	n.d.		96.9
164		T-2	red-p.	XIV	46.27	2.32	17.90	17.97	4.83	1.03	0.37	0.44*	3.79	0.12	0.40	0.06	n.d.	n.d.		95.1
106,164		T-3	blue	XIV	48.78	2.33	16.08	19.02	4.98	1.24	0.35	1.07*	3.83	0.17	0.26	0.04	n.d.	n.d.		97.1
164		T-4	red-p.	XIV	48.61	2.27	18.84	17.55	4.69	1.00	0.36	0.52*	4.33	0.14	0.32	0.01	n.d.	n.d.		98.1
106,164		T-5	br.-ye.	XIV	49.09	2.20	18.75	17.66	4.82	1.18	0.30	0.59*	3.97	0.15	0.18	0.00	n.d.	n.d.		98.3
106,164		T-6	br.-ye./red	XIV	48.69	2.36	18.10	17.84	4.99	0.98	0.43	0.44*	3.74	0.05	0.95	0.06	n.d.	n.d.		98.2
106		T-6	noc.	XIV	47.71	2.42	19.04	19.03	5.10	1.12	0.39	0.47*	4.40	0.15	0.12	0.04	n.d.	n.d.		99.5
164		T-7	br.-ye.	XIV	47.96	2.10	18.06	16.78	4.86	0.95	0.32	0.41*	3.87	0.13	0.04	0.09	n.d.	n.d.		95.2
164		T-8	blue	XIV	47.53	2.21	20.60	18.21	4.86	0.00	0.37	0.00	3.47	0.09	0.19	0.08	n.d.	n.d.		97.6
106		T-31	red	XIV	49.27	2.30	19.09	17.78	4.75	1.01	0.36	0.53*	4.39	0.17	0.32	0.01	n.d.	n.d.		99.5
106		T-31	noc.	XIV	48.97	2.27	19.10	17.37	4.62	1.00	0.35	0.54*	4.25	0.16	0.04	0.01	n.d.	n.d.		98.1
106		T-35	red	XIV	46.68	2.59	19.59	19.28	5.05	1.20	0.46	0.53*	3.88	0.18	0.44	0.09	n.d.	n.d.		99.4
106		T-35	noc.	XIV	43.42	2.48	21.41	20.78	4.74	1.34	0.58	0.58*	4.30	0.18	0.07	0.11	n.d.	n.d.		99.4
164	Santa Maria del Mar (Barcelona)	M-1	blue	XIV–XV	48.10	2.09	20.70	13.20	4.97	1.31	1.76	0.42*	5.18	n.d.	0.04	0.01	n.d.	n.d.		97.4
164		M-2	green	XIV–XV	47.74	1.93	17.21	13.42	4.52	1.12	1.29	0.52*	4.65	n.d.	3.58	0.09	n.d.	n.d.		95.6
164		M-2	noc.	XIV–XV	50.06	2.02	17.87	14.33	4.83	1.22	1.20	0.5*	5.31	n.d.	0.09	0.10	n.d.	n.d.		97.0
164		M-2	green	XIV–XV	48.37	1.88	17.13	13.50	4.51	1.04	1.25	0.57*	4.87	n.d.	3.75	0.00	n.d.	n.d.		96.3
164		M-2	noc.	XIV–XV	48.44	2.08	17.61	13.81	4.79	1.21	1.19	0.55*	4.91	n.d.	0.03	0.07	n.d.	n.d.		94.1
164		M-3	noc.	XIV–XV	49.21	1.93	20.55	16.59	3.15	1.11	0.27	0.53*	1.30	n.d.	0.62	0.70	n.d.	n.d.		95.4
164		M-3	red	XIV–XV	48.54	2.02	20.05	15.90	3.09	1.42	0.25	0.38*	1.64	n.d.	0.85	0.86	n.d.	n.d.		94.6
164		M-3	noc.	XIV–XV	49.14	1.90	20.49	16.52	3.15	1.28	0.24	0.27*	1.69	n.d.	0.05	0.83	n.d.	n.d.		95.3
164		M-4	blue	XIV–XV	52.60	1.81	18.80	12.70	5.03	0.78	0.95	0.51*	4.51	n.d.	0.16	0.01	n.d.	n.d.		97.4
164	Santa Maria de Pedralbes (Barcelona)	VP-2	noc.	XIV	46.75	1.19	25.24	17.72	3.50	0.70	0.27	0.39*	2.47	0.07	0.00	0.00	n.d.	n.d.		97.9
164		VP-2	red	XIV	45.31	1.46	22.70	20.40	3.13	0.71	0.25	0.38*	1.32	0.10	0.64	0.00	n.d.	n.d.		96.0

Table 1 continued

Ref	Site	Name/nb of samples	Color	Date	SiO_2	Al_2O_3	K_2O	CaO	MgO	MnO	Na_2O	Fe_2O_3/FeO*	P_2O_5	TiO_2	CuO/Cu_2O*/Cu**	PbO/Pb*	SO_2/SO_3*	Cl^-	Others	Tot.
164		VP-3	turquoise	XIV	48.38	1.13	23.26	19.01	3.22	1.07	0.11	0.51*	1.22	0.06	0.05	1.35	n.d.	n.d.		98.9
164		VP-4	blue	XIV	46.87	1.27	22.99	19.08	3.23	1.07	0.15	0.96*	1.15	0.10	0.21	1.06	n.d.	n.d.		97.2
164		VP-6	pink-Mn	XIV	47.98	1.45	23.93	17.94	3.65	1.41	0.19	0.46*	1.31	0.09	0.07	0.70	n.d.	n.d.		98.7
164		VI-21	noc.	XIV	55.51	2.26	16.79	14.04	4.27	0.89	0.54	0.41*	3.06	0.16	0.27	0.00	n.d.	n.d.		97.8
164		V-27	br.-ye.	XIV	55.98	2.23	16.87	14.17	4.29	0.89	0.43	0.41*	0.00	0.15	0.14	0.04	n.d.	n.d.		95.2
164		VI-34	pink	XIV	48.03	1.45	23.74	17.85	3.53	1.35	0.23	0.44*	1.04	0.08	0.04	0.72	n.d.	n.d.		98.1
164		CV-2	red-p.	XIV	53.90	2.28	16.84	14.08	3.48	0.90	0.48	n.d.	4.33	0.17	0.48	n.d.	n.d.	n.d.		96.9
38,165	Monasterio de la Cartuja de Miraflores (Burgos)	1	noc.	XV	59.10	1.37	4.57	23.52	3.72	1.07	2.85	0.50	1.15	n.d.	n.d.	n.d.	n.d.	n.d.	2.15	97.7
38,165		3	blue	XV	56.17	1.72	5.33	25.01	3.50	1.04	2.13	1.01	1.24	n.d.	n.d.	n.d.	n.d.	n.d.	2.70	98.1
38,165		5	noc.	XV	52.65	2.70	7.25	26.72	3.13	2.55	1.33	0.50	1.24	n.d.	n.d.	n.d.	n.d.	n.d.	1.93	99.6
38,165		7	noc.	XV	55.93	1.83	5.00	25.00	4.40	0.70	3.26	0.78	1.25	n.d.	n.d.	n.d.	n.d.	n.d.	1.85	100.0
166	Catedral de León	1	ocher + vi.	XIII	45.80	1.40	23.70	24.90	1.90	1.00	0.40	<LD	0.90	n.d.	<LD	<LD	n.d.	n.d.		100.0
166		2	red + noc.	XIII	54.40	1.70	16.80	14.80	2.60	1.60	1.40	1.20	5.50	n.d.	<LD	<LD	n.d.	n.d.		100.0
166		8	dark blue	XIII	54.10	2.90	6.20	29.20	1.50	1.20	0.60	1.50	2.80	n.d.	<LD	<LD	n.d.	n.d.		100.0
166		9	dark blue	XIII	50.30	1.60	18.80	14.30	4.20	2.10	0.80	1.40	6.50	n.d.	<LD	<LD	n.d.	n.d.		100.0
166		10	noc.	XIII	53.50	1.40	17.70	15.70	4.30	1.10	1.00	0.90	4.20	n.d.	<LD	0.20	n.d.	n.d.		100.0
166		11	vi.	XIII	49.90	1.30	19.80	15.60	4.10	2.50	0.90	1.00	4.90	n.d.	<LD	<LD	n.d.	n.d.		100.0
166		12	red + noc.	XIII	45.40	1.40	23.30	21.00	1.60	0.90	0.50	0.70	1.70	n.d.	<LD	1.30	n.d.	n.d.	2.20	97.8
166		16	green	XIII	45.10	1.30	24.50	22.90	1.80	0.70		1.80	1.20	n.d.	<LD	0.70	n.d.	n.d.		100.0
166		17	green	XIII	44.00	1.50	23.70	22.70	1.90	1.20	0.80	2.30	1.50	n.d.	<LD	0.40	n.d.	n.d.		100.0
166		18	green	XIII	45.00	1.90	22.70	21.20	2.00	0.40	0.70	2.30	3.10	n.d.	<LD	0.70	n.d.	n.d.		100.0
166		19	ye.	XV	51.60	1.60	18.40	16.40	3.20	1.40	1.00	1.10	4.60	n.d.	<LD	0.70	n.d.	n.d.		100.0
166		21	noc.	XVI	55.10	3.80	6.50	26.00	1.80	1.20	0.40	0.70	4.50	n.d.	<LD	<LD	n.d.	n.d.		100.0
166		22	vi. + noc.	XVI	44.30	2.10	23.00	22.70	2.50	1.10	0.80	1.00	2.50	n.d.	<LD	<LD	n.d.	n.d.		100.0
166		25	green	XVI	57.70	4.00	7.30	23.40	1.50	1.10	0.30	1.20	3.50	n.d.	<LD	<LD	n.d.	n.d.		100.0
166		26	green-ye.	XVI	54.20	4.10	8.60	25.60	2.00	1.00	<LD	1.50	3.00	n.d.	<LD	<LD	n.d.	n.d.		100.0
101		L1 (XRF)	light pink	XIV–XV	50.41	0.66	19.47	23.09	3.10	1.02	<LD	0.25	0.98	<LD	<LD	0.14	0.30	0.07	0.52	99.5
101		L1 (EDS)	light pink	XIV–XV	44.00	0.70	22.20	25.40	3.90	1.00	0.30	0.70	1.00	0.80	<LD	<LD	0.40	<LD		100.4
101		L2 (XRF)	red-f.	XIV–XV	45.68	1.22	24.10	19.91	2.60	0.78	0.77	3.20	0.62	<LD	0.03	0.26	0.23	0.06	0.53	99.5
101		L4 (EDS)	ye.	XIV–XV	45.50	2.30	20.00	14.90	8.10	1.30	3.20	1.10	2.80	<LD	<LD	<LD	0.30	0.50		100.0
101		L5 (EDS)	blue	XIV–XV	46.30	1.20	15.00	15.90	9.80	1.30	4.60	1.10	4.20	<LD	<LD	<LD	0.20	0.50		100.1
101		L6 (EDS)	red-f.	XIV–XV	43.60	2.80	24.50	21.10	3.90	0.90	0.60	1.00	1.10	0.20	<LD	0.20	0.10	<LD		100.0
101		L7 (EDS)	pink	XIV–XV	44.90	1.40	18.50	17.10	7.10	2.10	3.10	1.00	3.60	<LD	<LD	0.70	<LD	0.50		100.0
101		L8 (EDS)	vi.-flashed	XIV–XV	44.70	2.40	24.70	20.20	3.60	1.10	0.40	0.90	1.10	<LD	<LD	1.00	<LD	<LD		100.1
101		L9 (XRF)	greenish	XIV–XV	49.92	0.93	16.91	15.23	5.66	2.04	2.77	0.61	4.64	0.12	0.27	<LD	0.19	0.39	0.32	99.7
101		L9 (EDS)	greenish	XIV–XV	41.00	0.90	21.00	17.30	8.50	2.30	3.20	0.30	4.80	0.20	<LD	<LD	0.10	0.50		100.1
101		L10 (XRF)	ye.	XIV–XV	55.48	0.85	13.75	15.77	5.03	1.25	2.63	0.61	3.65	0.08	<LD	<LD	0.07	0.60	0.76	99.8
101		L10 (EDS)	ye.	XIV–XV	47.70	1.10	17.00	17.10	6.70	1.20	3.90	0.90	3.90	<LD	<LD	<LD	<LD	0.70		100.2

Table 1 continued

Ref	Site	Name/nb of samples	Color	Date	SiO_2	Al_2O_3	K_2O	CaO	MgO	MnO	Na_2O	Fe_2O_3/FeO*	P_2O_5	TiO_2	CuO/Cu_2O*/Cu**	PbO/Pb*	SO_2/SO_3*	Cl^-	Others	Tot.
101		L11 (XRF)	greenish	XVI	57.32	<LD	7.26	25.89	3.54	1.24	<LD	1.42	1.94	0.43	<LD	<LD	0.14	0.22	0.60	99.4
101		L11 (EDS)	greenish	XVI	45.40	4.20	9.60	28.50	4.90	1.20	1.30	1.50	2.30	0.80	<LD	<LD	<LD	0.30		100.0
	Italy																			
167	Certosa di Pavia	S. Cat. 8	noc.	XV–XVI	51.37	2.21	15.19	17.09	7.02	0.66	0.42	0.73*	4.35	n.d.	0.12*	n.d.	0.13*	0.27		98.6
167		S. Cat. 8	red	XV–XVI	51.39	2.52	14.01	16.49	7.45	0.72	0.34	0.74*	5.06	n.d.	0.73*	n.d.	0.05*	0.16		98.1
167		S. Cat. 8	noc.	XV–XVI	51.35	2.22	15.73	18.32	7.38	0.62	0.48	0.69*	2.63	n.d.	0.02*	n.d.	0.12*	0.27		99.0
167		S. Cat. 11	noc.	XV–XVI	51.99	1.27	17.91	13.42	5.84	1.26	2.15	0.3*	5.10	n.d.	0.06*	n.d.	0.13*	0.31		99.3
167		S. Cat. 11	red	XV–XVI	51.75	1.63	18.37	12.38	5.67	1.17	2.40	0.39*	4.65	n.d.	1.02*	n.d.	0.1*	0.25		98.3
167		S. Cat. 11	noc.	XV–XVI	52.49	1.17	17.59	13.31	5.84	1.17	2.05	0.28*	4.70	n.d.	0.01*	n.d.	0.12*	0.39		98.7
167		S. Cat. 13	noc.	XV–XVI	53.65	2.37	15.98	17.18	7.51	0.64	0.51	0.67*	<LD	n.d.	0.18*	n.d.	0.12*	0.26		98.1
167		S. Cat. 13	red	XV–XVI	51.74	2.58	14.35	17.15	7.60	0.78	0.33	0.7*	<LD	n.d.	0.74*	n.d.	0.06*	0.12		94.7
167		S. Cat. 13	noc.	XV–XVI	54.10	2.44	16.12	18.34	7.50	0.71	0.49	0.73*	<LD	n.d.	0.06*	n.d.	0.12*	0.28		100.0
167		S. Greg. 5	green	XV–XVI	56.78	2.77	12.50	18.56	6.12	0.59	0.70	<LD	3.79	n.d.	<LD	n.d.	0.31*	0.29		102.1
167		S. Greg. 5	green	XV–XVI	52.55	2.55	13.10	17.76	5.91	0.52	0.77	<LD	3.82	n.d.	0.08*	n.d.	0.36*	0.15		97.1
167		S. Greg. 5	green	XV–XVI	46.94	2.44	14.61	19.11	5.59	0.59	0.82	<LD	3.80	n.d.	<LD	n.d.	0.32*	0.18		94.1
167		S. Bern. 10	ye.	XV–XVI	52.58	1.25	17.53	13.61	5.65	1.25	2.38	0.26*	4.80	n.d.	<LD	n.d.	0.1*	0.38		99.4
167		Presepe 14	ye.	XV–XVI	51.32	2.06	20.35	13.31	5.02	0.98	1.46	0.41*	4.60	n.d.	<LD	n.d.	0.18*	0.27		99.4
167		S. Greg.	ye.	XV–XVI	50.87	2.77	15.12	17.54	5.39	1.37	0.65	0.58*	5.30	n.d.	0.01*	n.d.	0.06*	0.10		99.1
167		S. Greg.	ye.	XV–XVI	50.05	2.69	15.14	18.08	5.30	1.38	0.65	0.55*	5.50	n.d.	<LD	n.d.	0.07*	0.11		98.9
167		S. Greg.	ye.	XV–XVI	50.81	2.80	15.45	18.30	5.34	1.33	0.65	0.55*	4.35	n.d.	0.01*	n.d.	0.07*	0.10		99.1
112		S. Greg. - 3	ye.	XV–XVI	54.82	1.61	17.51	14.60	5.55	0.96	3.13	n.d.	n.d.	0.63	n.d.	n.d.	n.d.	n.d.		98.8
112		S. Greg. - 4	ye.	XV–XVI	54.72	1.56	17.35	14.77	5.63	1.03	3.17	n.d.	n.d.	0.64	n.d.	n.d.	n.d.	n.d.		98.9
112		S. Greg. - 5	ye.	XV–XVI	56.42	1.61	16.55	14.43	5.66	0.93	3.04	n.d.	n.d.	0.60	n.d.	n.d.	n.d.	n.d.		99.2
112		S. Greg. - 6	ye.	XV–XVI	56.91	1.58	15.85	13.96	5.72	0.96	3.07	n.d.	n.d.	0.54	n.d.	n.d.	n.d.	n.d.		98.6
168	Duomo di Pisa	Red8-5	red	XV	43.80	1.04	21.55	21.34	2.93	0.69	0.18	0.29*	1.07	<LD	0.03**	0.27*	0.26*	0.03		92.6
168		Red8-6	red	XV	42.45	0.99	21.91	21.25	2.98	0.74	0.18	0.3*	0.98	0.04	<LD	0.25*	0.21*	0.03		91.6
168		Red8-7	red	XV	43.71	1.04	21.95	21.79	2.98	0.74	0.12	0.27*	1.03	0.05	<LD	0.26*	0.27*	0.03		93.4
168		Red8-8	red	XV	43.15	1.02	21.85	21.07	2.84	0.77	0.21	0.25*	1.07	n.d.	0.04**	0.32*	0.33*	0.03		92.0
168		Red8-9	red	XV	40.90	0.91	22.47	21.28	2.51	0.78	0.13	0.25*	0.93	n.d.	<LD	0.28*	0.23*	0.03		89.9
168		Red8-10	red	XV	42.92	0.98	22.23	20.93	2.84	0.65	0.09	0.27*	0.99	n.d.	0.03**	0.26*	0.27*	<LD		91.6
168		Blu2-4	blue	XV	44.30	1.17	23.45	20.20	2.88	0.62	0.21	0.48*	0.89	0.05	0.10**	0.03*	0.2*	<LD	0.11	93.8
168		Blu2-5	blue	XV	43.16	1.17	23.17	19.40	2.81	0.59	0.19	0.52*	0.88	n.d.	0.10**	<LD	0.28*	0.03	0.05	91.4
168		Blu2-6	blue	XV	43.25	1.13	23.15	19.88	2.81	0.65	0.16	0.42*	0.82	n.d.	0.09**	0.04*	0.27*	0.03	0.06	91.9
168		Whi5-4	white	XV	46.65	0.71	21.56	20.36	3.01	0.52	0.11	0.28*	1.10	0.04	0.04**	0.03*	0.31*	0.03		94.1
168		Whi5-5	white	XV	45.31	0.70	21.98	19.44	2.82	0.53	0.13	0.2*	0.96	n.d.	0.06**	<LD	0.34*	0.06		91.9
168		Whi5-6	white	XV	45.29	0.73	21.63	19.72	2.91	0.55	0.12	0.33*	0.95	n.d.	0.03**	0.04*	0.3*	0.03		91.9
168		Pur1-5	pu.	XV	47.07	1.11	20.55	18.72	2.96	1.22	0.12	1.03*	1.15	<LD	0.14**	0.04*	0.23	0.04		93.2
168		Pur1-6	pu.	XV	46.40	1.11	20.31	18.45	2.88	1.33	0.10	0.93*	1.03	n.d.	0.09**	<LD	0.26	0.05		91.9
168		Pur1-7	pu.	XV	45.46	0.82	20.81	18.44	3.01	1.58	0.14	0.36*	1.23	n.d.	<LD	<LD	0.30	0.04		91.8

Table 1 continued

Ref	Site	Name/nb of samples	Color	Date	SiO_2	Al_2O_3	K_2O	CaO	MgO	MnO	Na_2O	Fe_2O_3/ FeO*	P_2O_5	TiO_2	CuO/Cu_2O*/ Cu**	PbO/Pb*	SO_2/SO_3*	Cl^-	Others	Tot.
168		Gre4-5	green	XV	44.11	1.43	20.36	21.21	3.05	0.46	0.30	2.24*	1.23	0.06	0.03**	0.13*	0.17	<LD	0.04	92.4
168		Gre4-6	green	XV	42.26	1.38	20.50	21.28	3.02	0.39	0.31	2.11*	1.30	n.d.	<LD	0.11*	0.26	<LD		90.7
168		Gre4-7	green	XV	42.56	1.34	20.09	21.04	3.03	0.40	0.29	2.26*	1.25	n.d.	0.04**	0.17*	0.20	<LD		90.2
168		Yel10-2	ye.	XV	42.41	1.19	22.95	20.44	2.88	0.59	0.20	0.32*	1.03	n.d.	<LD	<LD	0.25	<LD		91.9
168		Yel10-3	ye.	XV	42.63	1.18	22.69	20.60	2.89	0.63	0.30	0.32*	1.10	n.d.	0.03**	0.04*	0.31	0.03		92.4
168		Pur7-1	pu.	XV	42.68	1.04	23.36	20.03	2.97	0.68	0.14	0.29*	1.14		0.04**	<LD	0.29	0.03		92.4
168		Pur7-2	pu.	XV	42.99	0.97	23.72	19.05	2.94	0.65	0.13	0.29*	1.04	n.d.	<LD	0.03*	0.31	0.04		91.8
168		Pur7-3	pu.	XV	43.31	1.00	23.80	18.86	2.91	0.72	0.15	0.33*	1.10	n.d.	0.03**	0.05*	0.28	0.04		92.2
59	Certosa del Galluzzo (Florence)	2	blue	XIV	45.61	1.37	26.11	17.97	3.31	0.61	0.19	0.83*	n.d.	0.06	n.d.	n.d.	n.d.	n.d.	0.03	95.2
59		3	blue	XIV	46.48	1.66	23.87	18.83	3.41	1.19	0.21	0.58*	n.d.	0.03	n.d.	n.d.	n.d.	n.d.	0.05	95.7
59		4	pink	XIV	45.85	1.95	25.79	17.61	3.16	1.68	0.21	0.6*	0.87	0.06	n.d.	n.d.	0.44	n.d.	0.03	97.6
59		5	red	XIV	48.45	0.74	23.33	19.50	3.16	0.50	0.09	0.17*	0.98	0.07	0.77	2.33	n.d.	n.d.	0.70	100.4
59		10	ye.	XIV	47.78	1.08	24.09	18.79	3.58	0.27	0.23	0.36*	1.04	0.05	n.d.	n.d.	n.d.	n.d.	0.05	96.9
	France																			
24	Cathédrale de Tours	To2	green	XIV–XV	53.60	1.50	17.80	12.70	6.90	1.20	2.20	1.00	3.80	0.20	n.d.	n.d.	n.d.	n.d.		100.9
24	Cathédrale d'Evreux	Ev	red	XIII–XIV	54.70	0.70	15.30	17.30	3.20	1.50	0.70	<LD	5.90	<LD	n.d.	n.d.	n.d.	n.d.		99.3
39		Ev1b	noc.	XIV	52.98	0.73	16.93	13.40	7.33	1.33	2.49	0.31	4.15	n.d.	n.d.	<LD	0.20	n.d.		99.9
25		EV3	noc.	XIII	58.40	3.40	5.30	20.40	3.00	0.60	2.20	0.6*	3.10	n.d.	n.d.	n.d.	n.d.	n.d.		96.4
24	Abbaye Saint-Victor (Marseille)	SVJ	ye.	XII–XIII	48.30	2.90	15.10	16.00	6.00	0.60	0.70	1.20	4.10	0.20	n.d.	n.d.	n.d.	n.d.		95.1
24		SVI	noc.	XII–XIII	51.47	4.16	15.03	13.87	4.84	0.95	2.10	1.25	4.47	0.15	<LD	<LD	n.d.	n.d.		98.3
24	Cathédrale Notre-Dame-du-Bourg (Digne)	DB	blue	XII–XIII	50.00	2.60	17.80	15.60	5.30	0.90	0.90	1.10	4.20	0.20	0.13	0.05	n.d.	n.d.		98.6
24		DV	green	XII–XIII	52.44	1.66	16.51	15.46	5.10	0.70	1.10	0.70	4.10	0.20	1.55	0.19	n.d.	n.d.		98.0
24		DR	red	XII–XIII	52.98	2.07	17.48	17.46	4.84	0.91	0.43	0.55	4.27	0.23	0.36	0.02	n.d.	n.d.		101.2
24		Dvio	vi.	XII–XIII	49.95	2.04	17.43	17.54	5.34	1.92	0.93	0.80	3.37	0.20	0.05	0.01	n.d.	n.d.		99.5
24	Palais archiépiscopal (Rouen)	RVF	dark green	IX	58.50	2.20	12.90	12.90	5.00	0.80	1.40	0.50	2.90	0.40	2.43	0.23	n.d.	n.d.		97.5
24		RId	noc.	IX	59.28	2.25	13.44	13.26	4.63	0.67	2.17	0.61	2.50	0.29	0.00	0.01	n.d.	n.d.		99.1
24		RV	green	IX	55.80	1.20	14.80	13.90	5.10	0.70	1.70	0.56	2.00	0.10	0.98	<LD	n.d.	n.d.		95.9
39	Abbaye Saint-Ouen (Rouen)	OU2b	noc.	XIV	57.76	0.98	12.70	13.79	6.81	0.70	2.53	0.60	3.60	n.d.	n.d.	0.10	0.18	n.d.		99.8
39		Ou4b	noc.	XIV	54.64	1.33	17.05	12.34	6.80	1.09	1.89	0.66	4.52	n.d.	n.d.	<LD	0.26	n.d.		100.6
39		OU5a	noc.	XIV	53.61	1.30	16.73	11.73	7.03	1.02	2.59	0.76	4.50	n.d.	n.d.	<LD	0.28	n.d.		99.6
25	Eglise Saint-Thurien (Plogonnec)	PLOG	noc.	XVI	55.60	1.30	10.60	15.90	7.50	0.80	3.20	0.5*	3.80	n.d.	n.d.	n.d.	n.d.	n.d.		98.7
127	Sainte-Chapelle (Paris)	/ 12	n.d.	XIII–XIV	52.50	1.62	16.30	14.70	5.80	1.23	1.33	0.64	4.37	0.22	n.d.	n.d.	0.16	0.48	0.23	99.6
2		47-1	pu.	XIII	53.99	1.21	17.11	13.38	5.04	1.68	0.63	0.51	4.88	0.21	0.03	0.19	0.36	0.51	0.25	100.0
2		47-5 F	pu.	XIII	55.87	1.74	14.4	13.77	5.97	1.29	0.9	0.51	4.07	0.25	0.04	0.23	0.16	0.40	0.23	99.8

Table 1 continued

Ref	Site	Name/nb of samples	Color	Date	SiO_2	Al_2O_3	K_2O	CaO	MgO	MnO	Na_2O	Fe_2O_3/FeO*	P_2O_5	TiO_2	CuO/Cu_2O*/Cu**	PbO/Pb*	SO_2/SO_3*	Cl^-	Others	Tot.
127	Basilique Saint-Urbain (Troyes)	/ 4	n.d.	XIII–XIV	49.90	2.03	23.80	14.70	3.59	1.15	0.43	0.55	2.75	0.06	n.d.	n.d.	0.35	0.20	0.33	99.8
2	Cathédrale Saint-Pierre et Saint-Paul (Poitiers)	41 C	pu.	XII	59.95	2.03	14.89	12.59	3.63	1.35	0.85	0.58	2.92	0.25	0.01	0.07	0.26	0.4	0.21	100.0
2		41 F	pu.	XII	57.48	1.87	15.84	13.35	3.63	1.42	0.81	0.62	3.48	0.26	0.02	0.19	0.31	0.46	0.23	100.0
2	Cathédrale Saint-Etienne (Sens)	42-3	pu.	XIII	57.06	1.52	14.91	13.37	5.35	1.74	0.73	0.56	3.36	0.19	0.17	0.09	0.23	0.39	0.30	100.0
2	Cathédrale de Soissons	43-1	pu.	XIII	55.26	1.44	16.6	13.77	4.58	1.73	0.45	0.6	4.14	0.26	0.04	0.13	0.31	0.37	0.30	100.0
2	Cathédrale de Soissons or Basilique Saint-Quentin (?)	44-1	pu.	XIII	57.55	1.99	17.05	10.44	4.81	1.69	0.75	0.75	3.53	0.27	0.03	0.17	0.23	0.43	0.29	100.0
2	Cathédrale Saint-Etienne (Bourges)	44-2	pu.	XIII	57.49	1.5	15.67	12.74	3.91	1.95	0.75	0.56	3.72	0.19	0.02	0.21	0.48	0.45	0.33	100.0
2		47-8	pu.	XIII	56.31	1.45	15.38	13.65	5.35	1.81	0.68	0.55	3.6	0.18	0.02	0.05	0.19	0.39	0.36	100.0
2		47-25	pu.	XIII	55.02	1.35	17.95	12.6	4	1.44	0.51	0.53	5.11	0.18	0.02	0.09	0.46	0.4	0.32	100.0
2	Cathédrale Notre-Dame (Chartres)	42-2	flesh	XIII	57.9	1.7	13.24	13.9	5.13	1.5	1.66	0.62	3.01	0.23	0.02	0.04	0.25	0.53	0.26	100.0
2		43-2	pu.	XIII	57.6	1.78	12.66	14.46	4.98	1.63	1.76	0.65	3.15	0.23	0.04	0.10	0.19	0.45	0.29	100.0
2	Cathédrale Saint-Maurice (Angers)	47-10	flesh	XII–XIII	61.71	1.7	13.29	12.25	4.08	1.58	0.87	0.51	2.66	0.21	0.01	0.09	0.36	0.41	0.25	100.0
2		47-23	flesh	XII–XIII	60.56	1.59	13.46	12.59	4.49	1.52	0.96	0.49	2.99	0.2	0.01	0.16	0.33	0.39	0.24	100.0
2		47-17	pu.	XIII	56.67	1.71	14.61	14.01	5.61	1.96	1.24	0.53	2.28	0.16	0.07	0.15	0.25	0.35	0.36	100.0
2	Abbaye Saint-Germain-des-Prés (Paris)	42-5	noc.	XIII	59.42	2.21	13.79	12.96	4.55	1.2	0.74	0.81	2.76	0.28	0.10	0.14	0.27	0.35	0.37	100.0
2		44-3	noc.	XIII	60.04	1.21	14.37	11	6.55	1	1.62	0.4	2.27	0.13	0.20	0.24	<0.11	0.52	0.30	99.9
2	Eglise Notre-Dame (Dives-sur-Mer)	47-28	noc.	XIV	59.7	1.25	13.53	11.67	5.97	0.93	2.29	0.52	3.01	0.11	0.03	0.1	0.1	0.54	0.22	100.0
	GERMANY																			
24	Katharinenekirche (Oppenheim)	Op1	noc.	XIV	46.90	3.50	11.20	28.50	3.20	1.50	0.70	1.30	2.20	0.20	n.d.	n.d.	n.d.	n.d.		99.2
24	Meißner Dom	Me	green	XIV	48.10	1.00	22.40	19.40	3.20	0.60	0.20	1.30	1.70	<LD	n.d.	n.d.	n.d.	n.d.		97.9
127	Kölner Dom	I / 2	n.d.	XIII–XIV	48.80	1.90	21.00	19.10	4.00	1.53	0.30	0.49	1.90	0.09	n.d.	n.d.	0.2	0.07	0.25	99.6
127		II / 2	n.d.	XIII–XIV	44.70	3.00	10.60	28.50	3.97	0.95	0.30	0.55	3.80	0.13	n.d.	n.d.	0.09	<LD	0.90	97.5
	Austria																			
30	n.d.	/ 67	n.d.		53.60	2.70	16.80	18.60	3.40	n.d.	1.30	1.00	n.d.	n.d.	n.d.	n.d.	n.d.	n.d.		97.4
	United Kingdom																			
169	York Minster	/ 35	pink, green, amber, blue, red-f.	XII	55.90	0.80	12.50	15.30	9.40	1.12	1.80	0.15	2.50	n.d.	n.d.	0.05	n.d.	n.d.		99.5
169		/ 10	green, pink, amber	XIV	54.60	0.70	10.50	17.10	10.40	1.32	2.60	0.15	2.40	n.d.	0.05	0.04	n.d.	n.d.		99.9
169		/ 5	red-f., blue, green	XII	52.50	1.00	10.90	27.30	5.10	0.73	0.40	0.20	1.60	n.d.	0.12	0.07	n.d.	n.d.		99.9

Table 1 continued

Ref	Site	Name/nb of samples	Color	Date	SiO_2	Al_2O_3	K_2O	CaO	MgO	MnO	Na_2O	Fe_2O_3/FeO*	P_2O_5	TiO_2	CuO/Cu_2O*/Cu**	PbO/Pb*	SO_2/SO_3*	Cl^-	Others	Tot.
[169]	Canterbury Cathedral	/ 7	green, blue, red-f.	XII	53.10	1.00	11.00	23.90	6.20	0.87	0.20	0.20	2.50	n.d.	n.d.	0.03	n.d.	n.d.		99.0
[169]	Carlisle Cathedral	/ 10	green, blue, pink, amber	XIV	51.30	1.40	10.60	27.40	6.30	0.88	0.10	0.25	1.70	n.d.	0.01	0.02	n.d.	n.d.		100.0
	Total			Min	40.19	0.65	4.57	10.44	1.50	0.00	0.09	0.00	0.00	0.03		0.00	0.07	0.03		
				Max	61.71	4.20	26.11	29.20	10.40	2.55	4.60	3.20	6.50	0.80		2.15	0.48	0.70		
				Mean	50.15	1.77	17.56	17.82	4.52	1.07	0.95	0.83	2.95	0.19		0.25	0.25	0.26		
				Std	5.17	0.74	4.62	3.99	1.63	0.43	0.94	0.52	1.48	0.15		0.38	0.09	0.19		

The name of the sample or the number of samples (without name), as well as the color (when available) are indicated. n.d. means not described and <LD below limits of detection.
Colors: *br.* brown, *ye.* yellow, *pu.* purple, *red-f.* red-flashed, *red-p.* red-plaque, *vi.* violet, *noc.* colorless or uncolored.
* and ** refer to the corresponding oxide or element in the column title.

and mainly between 0.06 and 0.34 µm $year^{-1}$ when altered in atmosphere.

Secondary phases and deposits

Secondary phases such as salts are present on the surface or within cracks. Thus, the altered layer sometimes appears to be covered by a network of cracks filled with secondary phases, which can lead to the detachment of scales. During alteration, the released elements can react with elements from the environment, notably with SO_2 and CO_2 dissolved in the water or oxalates produced by microorganisms, to form mainly sulfates (e.g. gypsum, syngenite), carbonates (calcite) and oxalates (weddellite) (Table 2)[24,29,58]. Phosphates (brushite) can also be formed if the glass is rich in P[59]. Other components can deposit on the surface of the glasses (particulate matter such as soot, marine aerosols (e.g. NaCl), mineral dust, metallic fragments, pollens, etc.).

Exposure campaigns of model glasses over varying times in different environments show that the secondary phases are similar to those observed on ancient stained glass (mainly gypsum and syngenite) (see Tables 2 and 4).

The browning phenomenon of Mn glass

Some stained glass pieces present a severe change of their original color causing a loss of transparency and legibility of the artwork (e.g. Fig. 1g). Different kinds of physico-chemical processes can lead to a darkening of the surface of the stained glass: enrichments in Pb and Zn[60], presence of oxalates and melanin of biological origin[61] and presence of Mn-rich phases[62]. The browning phenomenon, strictly speaking, is associated with these Mn-enrichments observed in stained glass windows exposed to the atmosphere[62,63] and in archeological stained glass[44,45,64,65]. This phenomenon is characterized by brown spots and affects in particular the Mn-bearing glasses. In the case of atmospheric alteration, Mn originates from the glass, while in archeological context, it may have an external source (soil) and is usually associated with Ca, S, and P. Generally, Mn concentrates as small nodules or more extensive patches in fractures, craters, or near the surface[62,63,65]. The browning is then explained by an oxidation of Mn(II)/Mn(III) present in the glass introduced as a colorant or decolorizer[2,6,21] to Mn(III)/Mn(IV)[61,63,64,66] favored in alkaline environment. However, the determination of the valence and nature of the phases remains analytically complicated, as the oxidation state of Mn and its chemical environment can vary from sample to sample. In addition, the Mn-rich phases are small, amorphous or poorly crystallized and reactive[25,62]. Their precise identification remains an important challenge, as it would help to find safe and effective conservation-restoration treatments. The browning of the medieval glasses is a very damaging pathology for which there is a great expectation of solutions.

ALTERATION MECHANISMS

Reminder on glass alteration mechanisms

An extensive literature exists on glass alteration mechanisms[22,67]. Briefly, hydration consists first in the diffusion of water molecules or dissociated water molecules in the glass[68–71]. It depends on the topological constraints of the glass[72] and is associated to the dissociation of water molecules[73,74]. Then, hydration can be accompanied by the preferential release of modifier ions (especially alkaline elements) in solution. This mechanism is attributed to ion-exchange reactions (or interdiffusion) between

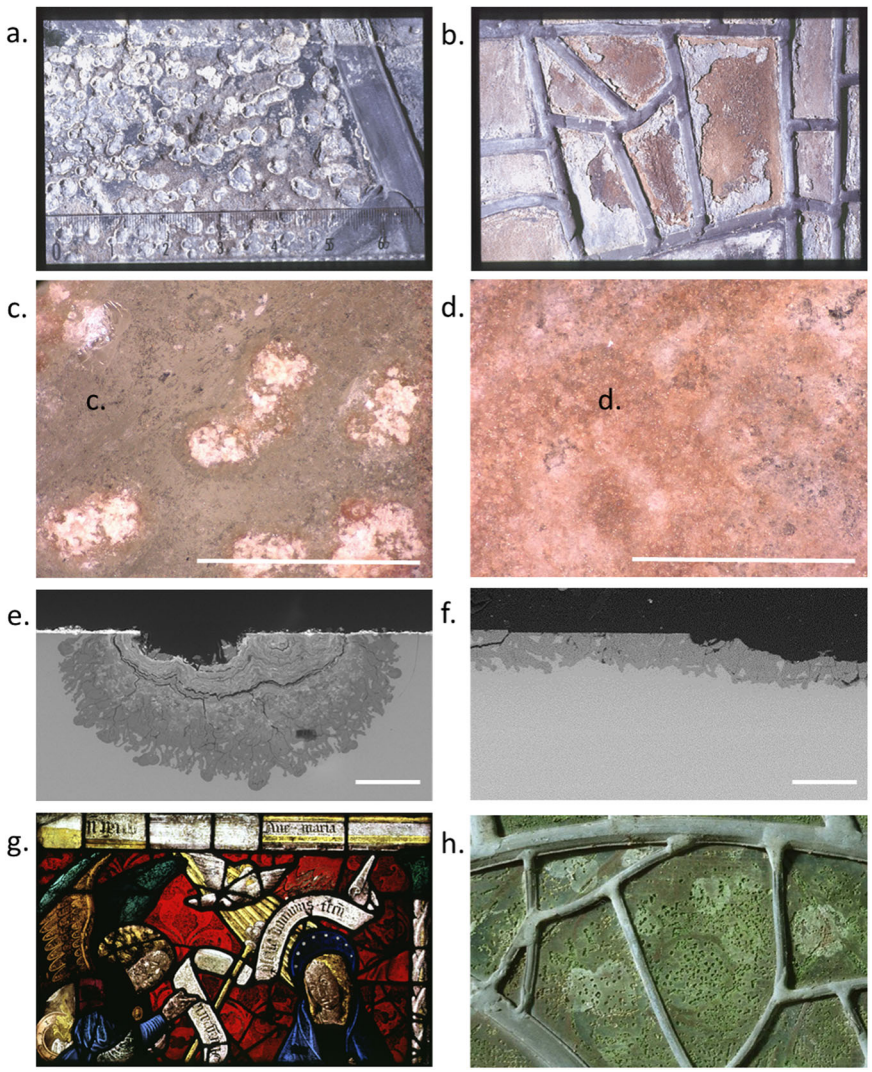

Fig. 1 Pictures of altered ancient stained glass windows. a, **b** are pictures of stained glass windows on their external faces coming from the Basilica of Saint-Remi in Reims (Marne) and dating from the twelfth century. The width of the leads is 6 mm. **c**, **d** are images in optical microscopy of Ou4, a stained glass window coming from the Abbey of Saint-Ouen in Rouen (Seine-Maritime) and dating from the fourteenth century: internal face with craters (**c**) and external surface with an opaque crust (**d**). White scale bars correspond to 1 mm. **e**, **f** are SEM (scanning electron microscope) images of a crater observed on Ev1, a stained glass window coming from the Cathedral Notre-Dame of Evreux (Eure) and dating from the fourteenth century (on internal face) (**e**) and of a more uniform altered layer with material loss of Ou4 (external face) (**f**). White scale bars correspond to 100 µm. **g** is a picture of a stained glass dating from the fifteenth century and located in the Notre-Dame Church of Les-Noës-Près-Troyes (Aube) that shows the opacification of the glasses owed to the oxidation of manganese. **h** is a picture of a stained glass in Chartres (Eure-et-Loir), dating from the thirteenth century with the development of microorganisms on the surface.

hydrogenated species of the solution and alkaline elements of the glass[75]:

$$\equiv Si - O - M + H^+ \rightarrow \equiv Si - OH + M^+ (\equiv \text{represents the silica bonds}) \quad (1)$$

$$\equiv Si - O - M + H_3O^+ \rightarrow \equiv Si - OH + M^+ + H_2O \quad (2)$$

$$\equiv Si - O^- M^+ + H_2O \rightarrow \equiv Si - O^- H^+ + M^+OH^- \quad (3)$$

With M an alkaline element: Na, Li, K,…

The hydrogenated species that diffuse within the glass can vary as a function of alteration conditions and glass composition[69,76–78] and even of alteration depth[79]. Whatever the nature of the exchanged hydrogenated species, the interdiffusion mechanism, due to the consumption of protons or the creation of hydroxyls in solution, causes an increase in pH and leads to the formation of a hydrated and dealkalized layer.

The hydrolysis of the glass network affects the bridging bonds (Si-O-Si, Si-O-Al, Si-O-Zr…) and attacks the silicate network:

$$\equiv Si - O - Si \equiv + H_2O \leftrightarrow 2 \equiv Si - OH \quad (4)$$

The release of glass elements by these different mechanisms can lead to the formation of alteration phases (alteration layer and secondary phases).

In the literature, there is a strong debate on the altered layer formation mechanisms in aqueous medium: either by interdiffusion and local hydrolysis/condensation reactions or by coupled interfacial dissolution–precipitation[67,80–83]. However, the involved mechanisms greatly depend on glass composition and alteration conditions.

In aqueous medium, the contribution of each mechanism depends on the progress of the reaction (time, open or closed system, glass surface/solution volume), on the solution composition, pH and temperature. In atmospheric medium, these

Table 2. Overview of the alteration observed on Si-K-Ca stained glass windows in the literature (patterns, secondary phases, thickness of the altered layer) from different sites (local names) sorted by country.

Country	Ref.	Site	Date	Alteration patterns	Secondary phases	AL thickness (µm)
Portugal	[33,60,170]	Mosteiro da Batalha	15–16th c.	Ext: blackening, loss of material, enrichment in Zn and Pb (grisaille)	Ca carbonates and oxalates	–
Spain	[106,163,164]	Catedral de Tarragona/Santa Maria del Mar (Barcelona)/Santa Maria de Pedralbes (Barcelona)	14–15th c.	Ext: pits, AL	Gypsum, syngenite, calcite, quartz, Ca oxalates	20–300
	[38,165]	Cartuja de Miraflores (Burgos)	End 15th c.	Ext: AL, pits, deposits / Int: pits	Gypsum	40–100
	[101,166]	Catedral de León	13–14th c. (removed during the 19th)	Ext: pits, AL / Int: pits	Gypsum, Ca oxalates, Ca carbonates	200–250 (pits) 1000–3000 (AL)
Italy	[112,167]	Certosa di Pavia	15th c.	Ext: cracks, pits, AL / Int: pits	Gypsum	70
	[168]	Duomo di Pisa	15th c.	Ext: AL	Gypsum, Ca oxalates	–
	[59]	Certosa del Galluzzo (Florence)	End 14th c.	Ext: pits, AL	Gypsum, syngenite, brushite, calcite, despugolsite	–
France/ Germany	[24,171,172]	Katharinenekirche (Oppenheim); Cathédrale de Tours; Meißner Dom; Cathédrale d'Evreux	13–14th c.	Int: pits / Ext: fractured AL (phases in the cracks parallel to the surface)	Sulfates (gypsum), carbonates	40–225 (ext)
	[173]	Cathédrale Notre-Dame de Strasbourg, Cathédrale Notre-Dame de Sées, Cathédrale Notre-Dame de Coutances, Cathédrale Saint-Corentin de Quimper	14th c. 14th c. 13th c. 16th c.	Ext: fractured AL	Gypsum	50 250 100–150 200
	[174]	Cathédrale de Tours	13th c.	Ext: AL	Gypsum, Ca oxalates	150
	[175]	Cathédrale de Tours	14th c.	Ext: AL	Sulfates (Ca, Cu)	500
	[175]	Cathédrale Notre-Dame de Strasbourg	14th c.	Ext: AL rich in Fe and Mn		500–1000
	[39,86,102]	Cathédrale d'Evreux; Abbaye Saint-Ouen (Rouen)	14th c.	Int: pits / Ext: pits or fractured AL, lamina, scales	Gypsum	0–230
Austria	[176,177]	Austrian sites	13–15th c.	Ext: pits, AL	Gypsum	50–150 (pits)
United Kingdom	[169]	York Minster, Canterbury Cathedral, Carlisle Cathedral	12–14th c.	Ext: fractured AL	Sulfates (Ca, Mg, Ba, K, Pb), calcite	–

Ext external face, *int* internal face, *AL* altered layer.

Table 3. Chemical composition (in wt%) of model glass (of cited references).

References	Name	SiO_2	Al_2O_3	K_2O	CaO	MgO	MnO	Na_2O	Fe_2O_3/FeO[a]	P_2O_5	TiO_2	others	Total
37,98,102,125,126,178	Si-K-Ca	50	2	25	18	3				2			100.0
88	SG1	52	2.4	22.6	17.7	3.3		0.4		1.6			100.0
88	SG2	54.7	2.2	20.6	15.6	3.5		3.4					100.0
36,85,91,140	SG3	51.3	1.8	19.2	16.8	4	1	1.1	1.2	3.8			100.2
29,31,136,147	M1 or MI	48	1.5	25.5	15	3		3		4			100.0
31,131,136	M3	60		15	25								100.0
128,179	Ca-K	53.67	0.83	18.77	21.57	3.3		1.53					99.7
127	SC	53	1.7	18	15	5.8	1	1		4.4			99.9
127	TR	51	2.3	24	16	3	0.8	0.5	0.5	1.9			100.0
127	CL_I	50.5	1.8	20.2	19	3.9	1.5	0.5	0.5	1.8			99.7
127	CL_{II}	46	3.5	11	30	4	0.5	0.5	0.8	3.7			100.0
30	Potash-lime	60		15	25								100.0
100	KCS	46.2	3.6	21.9	20.5	2.9		0.8		3.3	0.1		99.3
180	KCV	57.14	4.16	17.56	16.64	1.96		0.1	0.12	1.76	0.06	0.48[a]	100.0
111,147	M1.0	54.2		28.8	17								100.0
148	Glass 2	48.4	2.5	10.6	30.3	3.2	1.1	0.5		3.4			100.0
148	Glass 3	47.2	2.4	16.3	26	3.2	1.1	0.5		3.3			100.0
148	Glass 4	46.1	2.3	21.7	21.9	3.1	1.1	0.5		3.3			100.0
131	M I53.1	53.1	1	18	17.8	5		3.2		1.9			100.0
131	M 2.0	57.1		22.5	20.4								100.0
65,132	VK	52.19	2.39	14.9	14.9	4.9	0.76	1.8	0.7	3.34	0.24		96.1
133	GIC1	46.1	1.6	13.9	18.8	7.4	1.7	3		7			99.5
134	4	47.33	3.34	18.81	22.65	3.22	1.02	0.7	0.06	2.87			100.0
135,139	BMG	51		20.4	28.6								100.0
137	Type 3	53.02	2.5	17.8	14.22	4.21	0.91	0.55	0.99	3.47	0.14	2.17[b]	100.0
138	V1	61.11	1.99	12.29	18.5	3.82	0.03	0.38	0.15	1.67	0.09		100.0
138	V2	57.07	1.38	16.74	18.64	3.57	0.02	0.67	0.22	1.62	0.06		100.0
138	V3	53.1	0.73	23.49	17.53	3.24	0.02	0.26	0.09	1.52	0.03		100.0
113	VM	51.5	1.8	18.3	17.3	4.3	2.0	1.2		3.2			99.6
113	VNM	52.4	1.9	18.8	17.6	4.3		1.2		3.4			99.6

[a]Others are: SnO_2, CuO, SO_3, PbO.
[b]Others are: PbO, Cl, SO_3, CuO, ZnO, CoO, V_2O_3.

mechanisms have been less studied but they are similar to the continuous aqueous medium[84]. However, due to the changing conditions (rain events, T and relative humidity (RH) variations, pollutants, etc.), the kinetics and the respective contribution of each mechanism can vary[22].

Mechanisms can be studied and better understood by performing experiments in a real and monitored environment to focus on the first steps of alteration or by conducting laboratory experiments to control specific parameters. All these experiments have allowed to explain different alteration patterns and formation processes.

Properties of the alteration layer

Few studies have focused on the pore structure of the alteration layers of stained glass windows and on their transport properties.

Sessegolo[85] has performed gas adsorption measurements (see details in Supplementary Note 1). The analyzed sample is an ancient stained glass windows (fourteenth century) coming from the church of Rouen (France), of a size about $6 \times 4 \times 3\ mm^3$. It is altered on both the internal and external faces. The objective was to characterize the porosity of the external alteration layer. As the internal face was covered by pits and secondary phases, whose porosity can be different, this face was covered with epoxy resin. Moreover, two unaltered and polished (down to the quarter of micron) sample references (blanks) were also analyzed (one without preparation and one with a side covered with resin similarly to the stained glass sample).

Figure 2 shows that the stained glass stands out the blank samples with a significantly higher adsorption of N_2 ($1\ cm^3\ g^{-1}$ at standard temperature and pressure (STP) for the sample and $0.1–0.2\ cm^3\ g^{-1}$ STP for the blanks). This difference is due to the alteration layer developing a specific surface of $100–130\ m^2\ g^{-1}$. This wide range is due to the low value and the uncertainty about the mass of the alteration layer (calculated from geometrical considerations). This result is consistent with previous analyses from Sessegolo et al.[86]. The isotherm of nitrogen adsorption does not present any hysteresis, at the inverse of water adsorption[86], meaning that there is no capillary condensation in the mesopores. Therefore, the DFT (density functional theory) method can be applied to determine the pore distribution within the alteration layer.

Figure 3 clearly highlights the alteration of the stained glass compared to the blank (unaltered glass). A hybrid treatment was needed with a cylindrical geometry for the smallest pores (below 2 nm), whereas the majority of the porosity extends up to 15 nm according to a slit-shape geometry. The complex organization may suggest that the pore network evolves with initial cylindrical micropores that are progressively extended (slit geometry) by the

Table 4. Overview of the alterations (patterns and secondary phases) observed in exposure experiments of model glass in real atmosphere.

Reference	Time (months)	Alteration	Phases	Rate
		Sheltered from rain		
[31]	6–24	Deposits, irisations	Syngenite, gypsum, sylvite	N
[128]	3–12	Deposits	Sulfates	Y
[127]	4–12	Deposits, altered layer	Syngenite, gypsum	Y
[29]	6–12	Deposits, layer depleted in K	Syngenite, gypsum, carbonates, nitrates	Y
[178]	6	Deposits	K-Ca sulfates	N
[125,126]	0.5–12	Deposits, irisations	Sulfates, nitrates	Y
[98]	0.5–48	Deposits	Syngenite, gypsum, K carbonate	N
		Unsheltered		
[31]	6–24	Irisations, cracks, scales		N
[128]	3–12	Altered layer		Y
[30]	12–72	Altered layer		Y
[127]	4–12	Irisations, cracks, scales		Y
[37,125,126]	0.5–48	Loss of material, altered layer, irisations, cracks, scales, pits		Y
[180]	10–20	Pits, irisations, deposits		N
[161]	3–12	Pits, irisations, deposits		N

Model glass samples are Si-K-Ca glass (see Table 3 for composition) or ancient stained glass windows that have been repolished. The glasses are sometimes exposed with float glass for comparison. It is indicated if the alteration rate was measured (Y) or not (N).

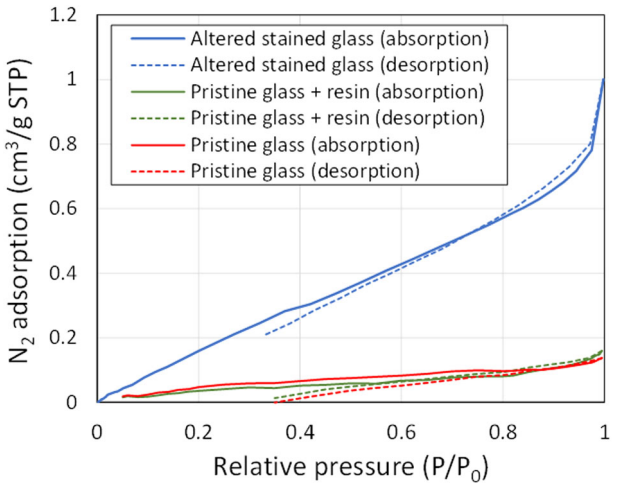

Fig. 2 N_2 adsorption isotherm on altered stained glass windows. The experiment was carried out on Ou2, a stained glass window coming from the Abbey of Saint-Ouen in Rouen and dating from the fourteenth century. The reference sample is a pristine model glass either covered by resin on one face, similarly to the internal face of the stained glass sample or not.

alteration. In the case of the unaltered glass, a slitted-shaped porosity is also observed. Its diffuse distribution and low intensity can be caused by the resin deposit.

Thus, the distribution of pore size shows a preponderant diameter of ~3 nm and a continuous decrease until 15 nm (Fig. 3). This result is consistent with previous analyses[86] that have obtained an average pore radius of 2 nm on a stained-glass window sample thanks to water adsorption isotherms (using a device IGAsorp®). The apparent diffusion coefficient of H_2O(g) in the pore network was 7.8×10^{-7} m^2 s^{-1}[86,87].

Alteration layer formation in aqueous medium

Verney-Carron et al.[88] have performed experiments on medieval-type model glasses (SG1 and SG2, see composition in Table 3) altered under dynamic conditions at 30 °C and pH 8 and pH 9 using solutions enriched in ^{29}Si (10 ppm). These conditions were chosen to simulate the formation of an altered layer of stained glass in contact with a residual water film, causing the pH to increase as well as the concentration of silicon in solution. Silicon isotopes were used to distinguish, within the weathering layer, between atoms originating from the glass (mostly ^{28}Si) and those originating from the solution (^{29}Si). The study of SIMS (secondary ion mass spectrometry) profiles shows that in these conditions, the mechanisms of formation of the altered layer are interdiffusion followed by local hydrolysis/condensation reactions.

Alteration layer formation in unsaturated medium (water vapor)

Apart from rain events, stained glass windows are altered by water vapor. Asay and Kim[89] have identified the structure of water adsorbed at the surface of silicon oxide at room temperature. Below 30% RH, a monolayer of water molecules is formed with an icelike structure. Between 30 and 60% RH, the liquid water thickness grows on top of the icelike structure. At RH higher than 60% RH, the thickness of the water film is significant and liquid water dominates. In these conditions, after sorption (and potential condensation at the surface or in pores), the alteration of glass by hydration[90] can occur.

Sessegolo et al.[91] have exposed medieval-type model glass (SG3, composition in Table 3) at different RH and temperatures values (20, 40, 70 and 91% RH at 20 °C and 55, 76, 83 and 95% RH at 50 °C) and durations (3 to 15 months). The alteration increases significantly at 95 % RH at 50 °C compared to lower RH.

At 20 °C, Sessegolo et al.[91] used water enriched with D and ^{18}O and at 50 °C only D. The comparison of the behavior of the different isotopes highlights that H and O isotopes are not correlated. From the SIMS profiles, it appears that D^+ and H^+ diffuse within the glass without O. The ^{18}O is only enriched at the extreme surface, which corresponds to the sorption and limited diffusion of water molecules. Therefore, the alteration of the glass seems mainly be governed by the hydration and the interdiffusion in unsaturated medium, driven by the H diffusion inside the glass matrix.

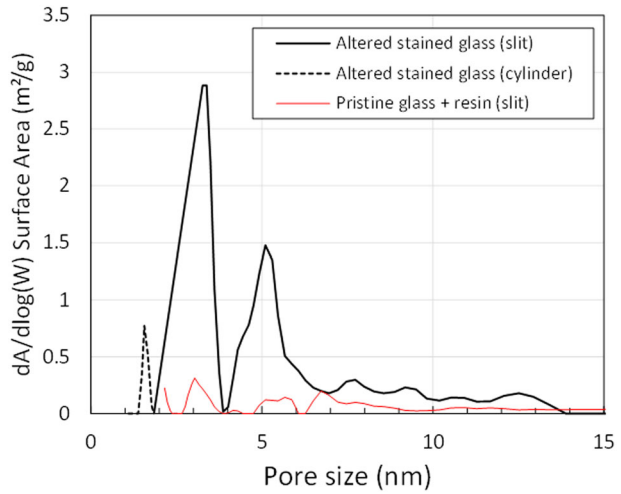

Fig. 3 Pore size (diameter in nm) distribution by surface area using DFT method on Ou2. This stained glass window comes from the Abbey of Saint-Ouen in Rouen and dates from the fourteenth century. The reference sample is a pristine model glass with one face covered by resin.

Sessegolo et al.[86] have also performed experiments with ancient stained glass samples (fourteenth century) exposed to 25 and 90% RH at 20 °C for 14 months. Vapor was enriched in ^{18}O and D to trace the circulation of water within the alteration layer and the reaction sites during the new phase of alteration. NanoSIMS mappings have shown D enrichments at the interface between pristine and altered glass but no ^{18}O enrichment. This indicates that the pursuit of alteration involves H^+ or D^+ diffusion (without O). This is consistent with the results obtained on the medieval-type model glass of Sessegolo et al.[91]. Moreover, similar results have been obtained in experiments with ^{18}O and D-enriched rainwater[87].

Sessegolo et al.[91] have also evidenced that the alteration mechanism can change with temperature. At 20 °C, SEM observations and SIMS analyses highlighted that the modifying cations K, Ca, Na and Mg are not leached during the alteration or only slightly on the surface. Hydration appears to be the main mechanism. The modifying elements remain within the altered layer and can migrate to the surface. Over time, ion exchange begins to appear. At 50 °C, the depletion of modifying cations is more marked, which is also reflected by the presence of salts on the surface (syngenite and Ca-carbonates). At this temperature, interdiffusion is predominant. Other studies also observed mainly hydration of glasses in unsaturated condition, including obsidian[92,93], mixed alkali glass[94], and commercial borosilicate glass[95]. Interdiffusion is observed for sodium glasses[93,96,97]. This behavior can be explained by the solvation properties of the ions and their mobility. The latter is low when the amount of water is low and it can vary depending on the ion (especially between Na and K). It would seem that hydration is favored for glasses poor in modifiers (obsidian), rich in aluminum and potassium. But this question would deserve to be dug.

Concerning the formation of pits, it seems that alteration is initiated from a specific zone, which could be a surface defect favoring the droplet condensation, microbubbles in the glass or the deposition of a salt particle. This can create a local environment. Gentaz et al.[98] highlighted the role of salts that form on the surface of glasses through experiments conducted on medieval-type model glasses (Si-K-Ca, composition in Table 3). In these experiments, different compounds (K_2CO_3, K_2SO_4 and $CaSO_4$) were deposited on glass surfaces, separately or together, and glass samples were subjected to cycles of relative humidity (between 33 and 97%) for 8 months. The presence of these salts induces the local formation of saline solution above their deliquescence point. This increases the contact with water, changes the pH of the solution and can then promote the dissolution of the glass. Moreover, the mixing of salts decreases the deliquescence point of the whole[99]. Similarly, Palomar et al.[100] performed weathering experiments on different glasses (including a Si-K-Ca glass, KCS, composition in Table 3) under unsaturated conditions in the presence of NaCl. The results were compared to samples altered in real atmosphere at a site near the Spanish coast. It was shown that NaCl has two effects. First, the crystals act as condensation nuclei in high humidity environments. The hydrated surface then favors the leaching of glass modifiers and the solubilization of atmospheric gases (CO_2, SO_2), resulting in the formation of various salts (sulfates, carbonates, chlorides). On the other hand, the presence of Na^+ ions can accelerate the alteration because the replacement of SiOH groups by SiONa generates an opening of the network. Palomar[101] has also highlighted the influence of glass composition (especially the Si content) on the alteration morphology. Pits are preferentially observed on glass with 60–65 wt% of SiO_2, whereas continuous alteration layer are visible on glass with 45–60 wt% of SiO_2.

Thus, the mechanisms of stained glass alteration are rather well understood. However, the wide range of chemical composition of glass according to the production areas and periods, the elaboration process (e.g. roughness, defects), as well as the diversity of environments in terms of climate and atmospheric composition induce variations in the observed patterns, from pits to the thickest layers. Furthermore, many mechanisms occur together and their respective contribution needs to be assessed.

Laminated alteration layers and scaling in atmospheric environment

Lombardo et al.[102] have studied the formation of laminae in the alteration layers of ancient stained glass windows and model glasses (composition in Table 3) exposed in real atmosphere for 3 years in unsheltered condition. On a fine scale, all the altered layers are made up of thin laminae (between 20 and 50 nm) that form blocks called laminations (of the order of µm) and marked by chemical heterogeneities on a micrometer or even nanometer scale (see an example on Fig. 1e). They also present a network of perpendicular or secant and parallel cracks. The secant cracks result from the humidity/drying cycles to which the glass is subjected and allow the transport of water to the interface between the altered glass and the pristine glass. Parallel cracks sometimes mark the separation of laminations. Secondary phases, such as sulfates, carbonates, phosphates and even silicates and metal oxides, are present within the cracks. From these observations, a scenario of alteration could be proposed[102]. First, interdiffusion leads to hydration and release of alkalis and alkaline earth elements. Beyond a certain thickness, a discontinuity is created, cracks appear favoring the transport of water, hydrolysis and local reorganizations in the form of laminae, as well as the precipitation of secondary phases from the elements of the glass and the environment (dissolved gases). These processes weaken the alteration layer and generate the propagation of new cracks and the formation of new laminae of potentially different orientation. Secondary phases will also precipitate in the voids caused by the cracks depending on the local conditions.

Stained glass weathering layers are also characterized by the presence of secondary phases, both on the surface and within the layer itself and by the formation of scales. Gentaz et al.[37] have exposed model glasses (Si-K-Ca, composition in Table 3) and pristine pieces of stained glass in urban atmosphere to rain over durations up to 48 months and characterized the alteration layers using profilometry and Raman spectroscopy. The alteration leads to the formation of a gel that fractures with changing hygroscopic conditions. Within the cracks that favor the access of water in

depth, the solution chemically evolves. The increase of the pH causes the dissolution of glass and the saturation of the solution leads to the precipitation of secondary phases such as calcite. The latter has a high crystallization pressure, which induces the detachment of the scales delimited by the network of cracks. Each scale has a thickness close to 4 µm.

BIOALTERATION AGENTS AND MECHANISMS

The presence of microorganisms (bacteria, fungi, algae, lichens) is commonly detected on the surface of stained glass windows (Fig. 1h). Stained glass may be a preferred habitat because its surface can be rough at a micrometric scale and the temperature/humidity conditions inside religious buildings are very compatible with the growth of microbial communities. As they are a potential source of nutrients (K, Ca, Mg, P, Fe, etc.), stained glass may also represent good nutritive substrates. The use of specific elements from the glass to sustain the development of microbial life makes the microorganisms potential participants in the alteration of stained glass, but their role is not completely clear and their significant impact still not evidenced.

The evolution of techniques now allows to better identify the microorganism species. Several approaches are possible: (1) culture of in situ microbiological samples and analysis of morphological, cultural (trophic type), metabolic, chemical characteristics, weathering potential, etc. However, only a small percentage (between 0.1 and 10%) of the microorganisms sampled in situ is cultivable in vitro; (2) metagenomic approaches (gene amplification, genomic probes, proteomics, sequencing) directly on in situ microbiological samples. Fungi are the predominant group present on stained glass[35,103]. It should be noted that *Aspergillus* and *Penicillium* which are very often identified[34,38,104] are extremely common fungi. They grow on decaying organic matter and are therefore very present in the environment. Rodrigues et al.[105] analyzed the DNA of fungi collected from stained glass windows in Portugal and cultivated and identified mainly Ascomycetes (with 5 genera *Alternaria*, *Chaetomium*, *Cladosporium*, *Didymella* and *Penicillium*) and Basidiomycetes (of the genus *Sistotrema*). Piñar et al.[106] also found species of the genera *Cladosporium* and *Phoma* on stained glass windows of churches in Catalonia. Corrêa Pinto et al.[107] analyzed Ascomycetes on modern stained glass in Brazil.

Bacteria are also observed on the surface of stained-glass windows. Piñar et al.[106] identified members of the phyla Proteobacteria, Bacteroidetes, Firmicutes and Actinobacteria. These bacteria are identical to those found on stone monuments. Marvasi et al.[108] characterized cultivable aerobic bacteria from a stained-glass window in the cathedral of Florence. Sequence analysis revealed the presence of the genera *Bacillus*, *Paenibacillus* and *Arthrobacter*. Valbi et al.[109] identified on different French stained-glasses several bacterial genera having weathering potential belonging to *Agrobacterium, Sphingomonas, Acinetobacter, Arthrobacter, Bacillus* and *Paenibacillus*. The *Arthrobacter* genus effect on glass alteration especially deserves further investigation.

The presence of some secondary phases can also be a tracer of the presence of microorganisms. From $\delta^{13}C$ analysis, Barbey et al.[63] suggested that 60% of carbonates had a biological origin. Similarly, Ca oxalates (weddellite, whewellite) are frequently observed on stained glass (see Table 2). They may be derived from the transformation of calcite into oxalate by reaction with oxalic acid secreted by microorganisms[110].

The influence of microorganisms on the mechanisms and rates of alteration is less clear. It is difficult to determine whether microorganisms are present on altered glasses because they represent a more favorable and protective environment (moisture, trapping of particles and organic matter in the crusts)[108] or whether they contribute significantly to alteration. Moreover, it is often tricky to discriminate between organic and inorganic chemical contributions. As an example, crater formation (biopitting) is very often attributed to microorganisms[103], but craters can also be formed abiotically[36,111]. In theory, microorganisms could have different effects: to accelerate the alteration by secreting different substances (organic acids, siderophores) and by forming a biofilm (sometimes colored) that creates a localized microenvironment and maintains a high humidity on the glass, to cause pH changes, to lead to the formation of craters and to create stresses or cracks (for filamentous organisms)[34,103,106,112].

If it exists now very powerful molecular approaches to screen the taxonomy and the diversity of the microbial population on stained glass, the possibility of cultivating only a small fraction of the living microorganisms limits the deep investigation of the bioalteration processes in laboratory experiments. However, the use of specific molecules that are known to be biologically produced or the design of experiments with pure bacterial strains, to target precise bacterial behavior, is a first lead to approach the occurring mechanisms. Valbi et al.[113] have performed abiotic dissolution experiments of VM and VNM model glasses (composition in Table 3) with siderophores that are molecules specifically secreted by some microorganisms to complex Fe and other elements such as Mn. They demonstrated the ability of these siderophores to increase the dissolution of the Mn-bearing model stained glass (VM). Valbi et al.[114] investigated the impact of *Pseudomonas putida*, a pure strain known for its ability to oxidize Mn, on the dissolution of the same model glasses. The addition of glass in the nutritive medium increases the bacterial growth as it provides nutrients. It can also trigger the production of siderophores if no iron is bioavailable. Moreover, the composition of glass can modulate biofilm formation. The presence of bacteria has no significant effect on the apparent glass dissolution rate, but the biofilm might retain a significant part of the dissolved elements, especially Si, Mn and P. In the future, further experiments in the presence of microorganisms are necessary to better understand the bioalteration processes caused by fungi and bacteria[105,107,115]. A particular interest should be dedicated to biofilms, as they develop at the interface between the glass surface and water. They are shown to accumulate elements and to represent very specific local reactive environments[116].

The key role of microorganisms has also been postulated in the browning phenomenon[103,110,117] but is not elucidated. For that, experiments have been carried out on model glasses in polluted atmospheres or in the presence of fungi or bacteria. Within the framework of the Franco-German research program for the conservation of historical monuments, Krawczyk-Bärsch et al.[66] observed significant Mn-enrichments in the alteration layer of Mn-rich model glasses when these latter were aged in presence of SO_2 and NO_2 that are assumed to favor the oxidation of Mn. On the opposite, lower Mn-enrichments are detected in the presence of fungi and bacteria. A browning was also observed on model glasses rich in Mn (1.5–2 wt% MnO) subjected to a polluted atmosphere (5 ppm of NO_x and SO_2) at 85% RH without bacterial intervention[61]. In other experiments glass samples have been immersed in Mn-rich solutions[111,118–120]. The Mn is found in the gel layer and in cracks and can form brown inclusions. Finally, Valbi et al.[114] experimentally formed brown Mn oxides (trapped in a thick biofilm) at the surface of a Mn-bearing model stained glass (VM), after only 7 days of incubation in a liquid culture of *Pseudomonas putida*. If these results encourage further investigations of the implication of some microorganisms in the browning pathology of stained glasses, there is still a long way to go in order to get clear evidence of the microbial contribution. The characterization of these brown phases and of their evolution over large timescales coupled with more identification work of the bacterial community living on stained glass surfaces and also the effect of the composition of the glass substrates is at least necessary to approach a conclusion.

ALTERATION KINETICS

Reminder on glass alteration kinetics

When a glass is altered in aqueous medium and in static condition, its alteration rate evolves over time and different alteration rate regimes can be distinguished. They were mainly described for the nuclear glass[15]. In the first stages of the alteration, there is a competition between interdiffusion and hydrolysis. This latter becomes predominant. The alteration is therefore congruent and the release of glass elements evolves linearly. Then, a drop in the alteration rate is observed that can be explained thermodynamically (by chemical affinity) and by the formation of a passivating altered layer. The residual rate corresponds to a low, but not null, alteration rate. It is controlled by the diffusion of elements through the gel layer and by the precipitation of secondary phases that sustains the alteration. In atmospheric medium, this evolution is less relevant as rains are episodic and the hygroscopic conditions highly variable. However, the initial dissolution rate can be measured in the laboratory to assess the alteration caused by rainwater. Also, the diffusion coefficients corresponding to the hydration or to the interdiffusion in aqueous medium or in vapor phase can be determined as a function of different environmental parameters. The alteration kinetics are actually controlled by the glass composition and by the environmental conditions.

Influence of glass composition

The terms "K-rich glass" or even "potassium-lime glass" or "calcium-potassium glass" mask a wide range of composition (Table 1) and therefore variations in terms of alteration rate. Newton[121] compared, for example, the degradation of a stained glass window containing 49.5 wt% SiO_2, 16.1% K_2O, 15.6% CaO from the twelfth century (highly altered) and that of a stained glass window of the same age with 54.0% SiO_2, 16.2% K_2O, 13.2% CaO (little altered). He explains this difference by the silica content, but also by the Ca concentration which, if too high, can make the glass unstable[122,123]. Palomar[101] has cataloged a large number of samples from the Cathedral of León in order to correlate alteration and composition. Therefore, there would be a lot of work to do to quantify the effect of the glass composition on the alteration rates[124].

This is especially true as the introduction of one element even low-concentrated in the glass can have a significant impact on the alteration rate. For example, Valbi et al.[113] highlighted that only 1 or 2 MnO wt% was enough to reduce by half the dissolution rate between two model glasses (VM and VNM) in water buffered conditions. Moreover, the Mn-bearing glass (VM) was more affected by the presence of metal-complexing molecules (such as oxalates) in solution, showing the importance of these minor elements in the silicate structure and their effect on dissolution behavior.

Therefore, various experiments will be compared in the following. But we have to keep in mind that the model glasses used in these experiments can be different and induce variations of alteration rate.

Kinetics determined from in situ exposures

The different experiments that have consisted in exposing Si-K-Ca glass in real atmospheres have been summarized in Table 4.

Sheltered environment. In sheltered environment, most of the experiments have only compared the nature of deposited or neoformed phases at the surface of the glass. In only some experiments[29,125–127], apparent weathering rates, corresponding to the K-depleted thickness divided by the exposure time (1 year) have been measured (see values in Table 5 and glass composition in Table 3). They are of the same order of magnitude (between 0.5 and 2.2 µm $year^{-1}$) depending on the sites. For these studies, the temporal evolution also shows that over a year, the alteration rate is constant or tends to slow down slightly. These rate values correspond to diffusion coefficients of the order of 10^{-20} m^2 s^{-1}. The chemical alteration of glass is therefore significant in sheltered condition. The comparison of hydration between sheltered and unsheltered conditions after 2 years of exposure shows that hydration is only 2.5 times higher for unsheltered condition, which highlights that the alteration caused by water vapor is not negligible relative to rain event and has to be considered to explain long-term alteration[126].

Unsheltered environment. For samples exposed to rain, it is more difficult to assess an alteration rate. Indeed, some authors give alteration thickness values[30,128] but the glasses could also have undergone dissolution and loss of material. Therefore, the apparent rates calculated from the thickness constitute the lower values that can be under-estimated (Table 5). The alteration rate varies between 0.4 and 5.4 µm $year^{-1}$ depending on the composition of the glass and the site. For the 20 sites of the ICP-Materials program[129], the thickness varies between 0.8 and 1.9 µm with an average value of 1.2 µm after 3 years[30], which corresponds to a rate of 0.3–0.6 µm $year^{-1}$.

As previously said, the observed alteration thickness results from diffusion kinetics but also from dissolution kinetics that can induce loss of material. Gentaz[125] measured mass losses over time on exposed samples: 2 mg cm^{-2} after 1 year, 4.5 mg cm^{-2} after 2 years, 7–8 mg cm^{-2} after 3 years and 9–11 mg cm^{-2} after 4 years. These values are consistent with the observation of the altered layer very affected by the loss of scales whose thickness is about 18 µm after 24 months, 30 µm after 36 months and 42 µm after 48 months (considering a density of 2.5 g cm^{-3}). It is thus tricky to combine dissolution and interdiffusion rates to assess the loss of material and the thickness of the altered layer[130].

Kinetics determined from laboratory experiments

Aqueous medium. In the aqueous phase, experiments have often aimed to simulate weathering phenomena under accelerated conditions (cycles, high temperatures, acidic pH) to compare them to atmospheric glasses[131,132], buried in the soil[133] or in the marine environment[134], from a phenomenological point of view (pits, scales, secondary phases). In some cases, it was to determine the influence of a parameter. Vilarigues and da Silva[135] have for example compared glasses altered in an agitated or non-agitated environment from FTIR measurements. They highlighted a more uniform morphology when the medium is stirred. De Bardi et al.[136] studied the effect of different acids on 2 glasses of different composition by IRRAS (infrared reflection absorption spectroscopy). Tournié et al.[137] and De Ferri et al.[138] determined the influence of the glass composition on the observed patterns and the nature of the secondary phases in H_2SO_4 at high temperature. Other studies have focused on the migration of metal ions in solution (Cu, Mn, Fe, Pb), potentially used as a dye or paint, within the weathering layer[111,139].

Experiments can also be performed to measure the weathering kinetics of stained glass in aqueous media[65,85,88,125]. From a set of experiments in diluted medium at different pH (between 2 and 11) and temperature (between 5 and 70 °C), Sessegolo et al.[140] have determined an initial dissolution rate (r_0) law for SG3 medieval-type model glass (composition in Table 3) following the equation:

$$r_0 = k \cdot [H^+]^n \cdot e^{-\frac{Ea}{RT}} \quad (5)$$

With k a rate constant ($k = 5.0 \pm 0.6 \times 10^6$ g m^{-2} day^{-1}), n an empirical pH-dependent coefficient ($n = 0.056 \pm 0.009$), Ea the activation energy ($Ea = 39.7 \pm 0.1$ kJ mol^{-1}), R the universal gas

Table 5. Alteration rates measured in exposure experiments of model glass in real atmosphere in sheltered and unsheltered from rain conditions.

Reference	Alteration thickness for different sites and exposure time	Alteration rate* (μm an^{-1})	D (m² s^{-1})
	Sheltered from rain		
[127]	Troyes: 0.2 μm at 4 months; 0.35 μm at 8 months; 0.5 μm at 12 months	0.5	0.6×10^{-20}
	Cologne: 0.55 μm at 4 months; 0.80 μm at 8 months; 0.90 μm at 12 months	0.9	2×10^{-20}
[29]	Athens (7 racks): 0.33–0.98 μm at 6 months; 0.85–1.57 μm at 12 months	0.9–1.6	$2–6 \times 10^{-20}$
	Krakow (7 racks): 1.13–1.83 μm at 6 months; 1.52–2.16 μm at 12 months	1.5–2.2	$6–12 \times 10^{-20}$
	London (7 racks): 0.68–1.27 μm at 6 months; 0.99–1.57 μm at 12 months	1.0–1.6	$2–6 \times 10^{-20}$
	Prague (7 racks): 0.49–0.96 μm at 6 months; 0.73–1.64 μm at 12 months	0.7–1.6	$1–7 \times 10^{-20}$
	Roma (6 racks): 0.36–0.77 μm at 6 months; 0.39–1.09 μm at 12 months	0.4–1.1	$0.4–3 \times 10^{-20}$
	Riga (2 racks): 0.89–1.06 μm at 6 months; 0.84–1.50 μm at 12 months	0.8–1.5	$2–6 \times 10^{-20}$
[125]	Paris: 0.05 μm at 1 months; 0.12 at 3 months; 0.31 at 4 months; 0.48 at 6 months; 0.59 at 8 months; 0.6 at 9 months; 0.7 at 12 months; 0.85 at 15 months; 1.2 at 36 months	0.7	1.2×10^{-20}
	Unsheltered		
[128]	Paris: 1.4 μm at 6 months; 1.8 μm at 9 and 12 months	1.8–2.8	
[127]	Saint-Urbain basilica (Troyes): 0.9 μm at 4 months; 2.0 μm at 8 months; 2.4 μm at 12 months	2.4–3.0	
	Sainte-Chapelle (Paris): 0.35 μm at 4 months; 0.4 μm at 8 and 12 months	0.4–1.1	
	Cologne Cathedral: 1.8 μm at 4 months; 2.4 μm at 8 months; 2.8 μm at 12 months	2.8–5.4	

From measured thickness and alteration duration, two rate values were calculated: an apparent alteration rate* after 12 months (in μm year^{-1}) and a diffusion coefficient D (see Eq. (7)) at 12 months.

constant ($R = 8.314$ J mol^{-1} K^{-1}) and T the temperature in K.

Classically, the initial dissolution rate law as a function of pH follows a U-shape for many glasses[141–145]. Yet for Si-K-Ca stained glass, the rate decreases slightly from acidic to basic pH. This behavior was previously observed by Sterpenich[65]. It is also similar to that of basic silicates (Schott et al.[146] and references therein). The dissolution of multi-oxide minerals and natural glasses requires the breaking of different types of bonds involving exchange reactions between protons and metals and occurring at different rates as a function of their relative strength. Generally, at acidic pH, the monovalent metal-oxygen bond is faster to break than divalent, then trivalent and last Si-O bonds. For aluminosilicate glasses, the hydrolysis of Si-O bonds that completely dissolves the glass network is thus preceded by the breaking of Al-O bonds and this exchange reaction is rate-limiting. This leads to a dependence on pH that is similar between the dissolution rate of the glass and the solubility of Al oxides or hydroxides. For a glass poor in Al and rich in Ca, and probably at high pH, the hydrolysis of Si-bonds is preceded by the breaking of Ca-O bonds. As the solubility of Ca and Mg hydroxides decreases with pH, the dependence on pH of Si-K-Ca glass could have a similar trend.

Verney-Carron et al.[88] have measured on relatively similar model glass samples (SG1 and SG2, composition in Table 3) dissolution rate values of 0.3–0.4 g m^{-2} day^{-1} at 30 °C and pH 9 and of ~0.6 g m^{-2} day^{-1}at 30 °C and pH 8. The values deduced from Eq. (5) at the same temperature are relatively close: 0.23 g m^{-2} day^{-1} at pH 9 and 0.26 g m^{-2} day^{-1} at pH 8. Differences could be explained by small differences of composition. Gentaz[125] have measured a value for Si-K-Ca glass (composition in Table 3) of 0.45 g m^{-2} day^{-1} in ultrapure water and at 20 °C. This is higher than the rate deduced from Eq. (5), i.e. 0.20 g m^{-2} day^{-1}, but the composition of glass is also different and less durable (Table 3). Values measured by Sterpenich[65] for VitK (composition in Table 3) are lower by a factor 2 to 25 probably for the same reasons. This points the key role of the composition that remains to be investigated more systematically.

The rate drop being partly controlled by the progressive increase of the concentration of silicon in solution and the altered layer being essentially composed of silica, the saturation indices of the solution with respect to siliceous phases have been calculated[140]. The dissolution rate drop can thus be described by a chemical affinity term:

$$r = r_0 \cdot \left(1 - \frac{Q}{K}\right) \tag{6}$$

With Q the ion activity product ($Q = (SiO_2(aq))$) and K the solubility constant (of amorphous silica $K_{SiO_2(am)}$).

The experiments of Sessegolo et al.[140] have also allowed to deduce diffusion coefficient for each experiment by using the second Fick's law:

$$e = \frac{NL(K)}{\rho} = 2\sqrt{\frac{Dt}{\pi}} \tag{7}$$

With $NL(K)$ the normalized mass loss relative to potassium, ρ the density of the glass (2.56 g cm^{-3} for SG3[140]) and t the time.

This has led to the implementation of a diffusion rate law as a function of T and pH:

$$D = D_0 \cdot [H^+]^{n'} \cdot e^{-\frac{Ea'}{RT}} \tag{8}$$

With D_0 an initial constant ($D_0 = 2.4 \pm 0.3 \times 10^{-10}$ m² s^{-1}), n' an empirical pH-dependent coefficient ($n' = 0.25 \pm 0.02$) and Ea' the activation energy ($Ea' = 34.5 \pm 0.3$ kJ mol^{-1}).

During these experiments[140], the weathering layers were also characterized after 70 days. The results show that at pH higher than 9, the dissolution is congruent, which can lead to the formation of craters but no alteration layer is observable at the SEM scale. For lower pH, the surface becomes rough and the alteration layer is more or less continuous. The more acidic the pH, the thicker the alteration layer. At pH 3, the alteration layer appears very scaly and cracked. Overall, the analyses show that the altered layer is very strongly depleted in K, while Ca remains relatively present. Its retention may be caused by the formation of several Ca-rich phases, such as hydroxylapatite and calcite. Aluminum and iron are insoluble and are therefore retained.

Unsaturated medium. Several series of experiments were performed in the laboratory in vapor phase to understand the role of

Table 6. Overview of laboratory experiments in simulated atmosphere (cf. Table 3 for model glass composition).

Reference	Glass	Time	T° in °C	HR in %	Gas concentration
[147]	M1.0/MI		20–45	72–97	SO_2 3 ppb–5 ppm
[148]	G2/G3/G4	400 cycles (of 7 h)	60 (3 h) + UV/−15 (4 h)	80 (3 h)/30 (4 h)	
		95 cycles (of 24 h)	40	100	SO_2 10 ppm–1800 ppm
[149]	M1	48–500 h	ambient		SO_2 0–0.1–1.1 ppm + dusts (Kopisty)

climatic factors or gaseous and particulate pollutants or to study the mechanisms and determine the rates (Table 6). The conditions are rarely realistic. Gas-phase experiments show that weathering increases with RH but is very low below 70%, suggesting the existence of a threshold[147]. Alteration also increases with SO_2 content[147,148]. Carbonates are formed at first and then sulfates. The quantity of secondary phases increases in the presence of dusts[149].

Few studies have measured the diffusion rate as a function of time, temperature and RH. Sessegolo et al.[91] have performed experiments at different RH values (between 20 and 95% RH), at 20 and 50 °C, with water vapor doped in D and in some cases in ^{18}O and for 3 to 15 months. They reported that the hydration thickness increases exponentially with time, similarly to Alloteau et al.[150] for historic glasses, whereas Cummings et al.[96] for Si-Na-Ca glass and Bouakkaz[151] for nuclear glass observed a square-root temporal evolution. This makes difficult the calculation of a corresponding diffusion coefficient.

Different studies conducted on various glasses at different RH values have found activation energies ranging between 34 and 138 kJ mol^{-1}[92,93,95,152–155]. However, these variations are supposed to depend on the glass composition, RH and studied species (H or O). Moreover, the change of the predominant mechanism (hydration/interdiffusion) as a function of temperature questions the relevance of the activation energy determination from Arrhenius' law[91,150].

The evolution of the diffusion rate as a function of RH is also variable. Several authors[91,152,156] observed a linear evolution until a threshold and then a sudden increase at high RH. However, for Morija and Nogami[154] and Cummings et al.[96] the hydration rate increases linearly from 5 to 100% RH.

More data are required to parameterize kinetic laws as a function of temperature and relative humidity. Also, in the context of stained glass alteration, the composition of the atmosphere has to be considered.

Programs such as MultiAssess or ICP-Materials provide some trends on the impact of the environment[129,157]. For example, after 3 years of exposure in unsheltered conditions in 24 different sites (ICP-Materials program), the altered layer (depleted in K) of model glasses close to medieval stained glass varies between 0.8 and 1.9 µm (i.e. a factor of 2.3) for very variable environments: average temperatures ranging from −0.8 to 24.2 °C, average RH between 57.5 and 84.3%, cumulative precipitation over 3 years from 618 to 5032 mm, SO_2 contents between 0.2 and 35.2 µg m^{-3} and NO_2 between 1.4 and 79.1 µg m^{-3})[30]. The highest thickness corresponds to the wettest site. Similarly, during the MultiAssess project, model glasses were exposed under sheltered conditions for 1 year in 6 sites (Athens, Krakow, Rome, London, Prague, Riga)[29]. Thicknesses ranged from 0.51 µm in Rome ($[SO_2] = 1.3$ µg m^{-3}, $[NO_2] = 14.4$ µg m^{-3} and $[O_3] = 52.8$ µg m^{-3}, T = 15.8 °C, RH = 72.1%) to 1.83 µm in Krakow ($[SO_2] = 19.9$ µg m^{-3} and $[NO_2] = 30.4$ µg m^{-3}) and $[O_3] = 62.2$ µg m^{-3}, T = 7.9 °C, RH = 74.7%). The thicknesses seem to be correlated with SO_2 and NO_2 concentrations but following non-linear relationships (regular increase until a threshold of about 10 µg m^{-3} for SO_2 and 30 µg m^{-3} for NO_2 and then a plateau). In view of these results, the variety of climates and pollution levels induces a factor of 2 to 4 of variation, which is relatively limited but has to be considered for a more refined modeling. The impact of climate and pollution is higher for M1 glass exposed in the ICP-Materials program in sheltered conditions. After 1 year, the alteration thickness varies between 1.6 and 22.1 µm[158].

The kinetic role of the alteration layer

When an alteration layer is formed, its passivating properties can control the alteration rate. This passivating role has been highlighted for nuclear glasses[159]. The altered layer can act as a molecular sieve and its porosity can become more and more closed. For stained glass, the morphology of the altered layer is particularly heterogeneous and unstructured due to the atmospheric medium that is multiphase and changing. These variations and the precipitation of hygroscopic salts at the surface and within the altered layer lead to mechanical stresses, cracks and loss of scales. All these open spaces permit the circulation of water (liquid or vapor) until the alteration front. In these conditions, the passivating role of the alteration layer can be questioned.

To address this issue, experiments using isotopic tracers (D and ^{18}O) have been carried out by simulating atmospheric cycles with rain events or an unsaturated atmosphere[86,87]. In both studies, ancient stained glass windows (fourteenth century) from the Notre-Dame Cathedral in Evreux (Ev1) and the Saint-Ouen Abbey in Rouen (Ou2) with a substantial alteration layer (~100 µm thick) were used. In the first study (saturated medium[87]), these stained glass samples were subjected to 13 cycles with 1 day of drizzle (synthetic rain rich in D and ^{18}O) and 6 days of drying. The temperature has varied between 22 and 32 °C and the relative humidity between 75 and 80% during the dry episodes. The samples were analyzed using Nano-SIMS mappings on cross-sections. The results show that the solution rapidly circulates by diffusion within the altered layer, both through the pores and the cracks. Moreover, an enrichment in D is observed at the interface between the pristine and the altered glass. It was assumed to be caused by the pursuit of the alteration during the experiment, superimposed to the centenary alteration. By measuring the thickness of the D-enriched zone, considering the time of the experiment and using Fick's second law (Eq. (7)), it was possible to calculate a diffusion coefficient corresponding to the exchange of ions between the protons and the alkalis. The value of the diffusion coefficient is 2.8×10^{-18} m^2 s^{-1} (for an average temperature of 25 °C).

In unsaturated medium, stained glass samples have been exposed to water vapor enriched in D and ^{18}O at RH between 25 and 90% and at 20 °C[86]. The Nano-SIMS mappings show that the isotopic ratios measured in the altered layer are higher than the natural abundances, highlighting the circulation and the homogeneous adsorption of water within the altered layer. Furthermore, significant deuterium enrichments at the pristine/altered glass interface allowed to calculate the corresponding diffusion coefficients: 3.6×10^{-20} m^2 s^{-1} at 70% RH and 4.9×10^{-20} m^2 s^{-1} at 90% RH at 20 °C. These values are similar to those measured on short-term altered model glasses in real atmosphere (Table 5). Therefore, this study emphasizes that the altered layer does not

limit alteration because its destructured morphology favors rapid transport of aqueous species to the weathering front.

ALTERATION SCENARIO OF THE ANCIENT STAINED GLASS WINDOWS

Mechanisms

Six or seven hundred years ago, a stained glass window was installed on a religious building. Since then, the stained glass is subjected to the action of water in vapor form and to more or less frequent episodes of rain depending on its location. During the unsaturated phase, hydration and/or interdiffusion are the predominant mechanisms. The kinetics of these processes depend on the relative humidity because this parameter defines the quantity of water molecules adsorbed and available for diffusion. Initially, it seems that it is H^+ that diffuses, opening the way to water molecules. Occasionally, the rain occurs. The immersed environment induces a greater alteration than the unsaturated environment. When it rains, the glass is in contact with liquid water, which can lead to the concomitant dissolution and interdiffusion. The contribution of these mechanisms depends on the pH and the composition of the solution. Moreover, a mixed effect of saturated/unsaturated exposures exists. Glass leaching on contact with liquid water is favored by prior exposure to relative humidity. Indeed, some elements are mobile but are not necessarily leached during hydration or interdiffusion in the vapor phase. They can be mobilized by rain events.

When the rainy episode ends, the glass remains wet. The composition of the residual water on the glass surface varies rapidly: Si concentrations will rapidly increase, decreasing the alteration rate by chemical affinity.

These alteration mechanisms lead to possible material losses and to the formation of an altered layer by interdiffusion and hydrolysis/condensation reactions. This layer is porous, with a pore radius of 1.5–2 nm on average and a distribution extending to 15 nm[86]. The pores constitute water reservoirs when the layer is soaked but also when the relative humidity is higher than 57% (threshold determined by Kelvin's equation for a pore radius of 2 nm, see below). Thus, outside of rain events, the layer is partially saturated with water.

In some cases, the alteration progresses in the form of craters. These are rather observed on the internal face or in the first stages on the external face and can afterwards coalesce to form a continuous layer. We can therefore assume that they are less exposed to rain (at the borders of windows for example). Their formation can be explained by the presence of surface defects (scratches) or aerosol deposits that favor the condensation of a water drop. The initiation of the alteration can be reinforced by an accentuation of the roughness[36], by the development of a porous and water-soaked altered layer (because of the condensation of water in the pores that maintains humidity) and the release of cations which precipitate as salts whose deliquescence can be aggressive[98]. However, the increase of the pH will only favor a weak dissolution[140]. Added to the silica saturation of the solution, this gives a preponderant place to interdiffusion. This results in deeper craters with a thick alteration layer. The role of microorganisms in the process remains to be clarified in the future. For glasses more subjected to rain, the weathering layer is more continuous on the surface.

On the long-term, the alteration of the glass continues. The weathering layer cracks due to hygroscopic variations and stresses exerted by the precipitation of secondary phases within it. It can also lead to the loss of scales when the alteration reaches a significant thickness. The cracks can constitute preferential paths for water up to the interface with the pristine glass and privileged zones of the alteration progression. Nevertheless, the formation of the weathering layer imposes a diffusive transport of water within it and limits the direct leaching, even if it does not have strictly speaking a passivating role. Since the network is mesoporous, it is essentially Knudsen diffusion, controlled by particle/wall collisions[86,160]. Therefore, the dissolution rate is slowed down over time and interdiffusion persists at a rate that depends on the square root of time and varies with relative humidity.

Kinetic modeling

Simulating the alteration for 700 years is complex. It requires to consider the alternation of phases saturated (rainfall events) and unsaturated in water, as well as transitory states that can favor evaporation and precipitation or inversely deliquescence of salts. A geochemical model based on kinetic laws parameterized as a function of climatic parameters and atmospheric pollutants could allow to predict the alteration of stained glass windows in the context of the climate change and pollution evolution. Here, the objective is to account for the alteration over centuries and assess if the extrapolation of short-term kinetics is consistent with the observations carried out on ancient stained glass samples. As stated above, the alteration thickness of medieval stained glass windows mainly ranges between a few and 300 µm, which corresponds to diffusion coefficient (according to Eq. (7)) of ~10^{-21} to $3.5{\cdot}10^{-18}$ $m^2\,s^{-1}$.

The alteration can occur in three different situations: rainfall events, residual or pore water in the alteration layer and water vapor. Therefore, the altered layer thickness (ALT) results from these three situations and their associated kinetics:

$$\mathrm{ALT} = 2\sqrt{\frac{D_{\mathrm{rain}} \cdot x_{\mathrm{rain}} \cdot t}{\pi}} - \frac{r \cdot x_{\mathrm{rain}} \cdot t}{\rho} + 2\sqrt{\frac{D_{\mathrm{wet}} \cdot x_{\mathrm{wet}} \cdot t}{\pi}} + 2\sqrt{\frac{D_{\mathrm{vapor}} \cdot x_{\mathrm{vapor}} \cdot t}{\pi}} \quad (9)$$

With D_{rain} the diffusion coefficient of glass modifier elements during rainfall events that depends on pH and T (Eq. (8)), x_{rain} the proportion of rain time, t the time of alteration, r the dissolution rate (Eqs. (5) and (6)), ρ the glass density, D_{wet} the diffusion coefficient of glass modifier elements when water fills a significant part of the porous network of the altered layer that also depends on pH and T (Eq. (8)), x_{wet} the fraction of time of altered layer imbibition, D_{vapor} the diffusion coefficient of glass modifier elements when water is as vapor, x_{vapor} the fraction of time of water as vapor $(1 - x_{\mathrm{rain}} - x_{\mathrm{wet}})$.

During rainfall events, interdiffusion and dissolution can occur. Kinetic laws (Eqs. (5), (6) and (8)) allow to calculate the alteration thickness due to interdiffusion (1st term in Eq. (9)) but dissolution can induce a loss of material (2nd term). The 3rd term corresponds to the alteration caused by interdiffusion when the altered layer remains wet (after rain events or at high RH) and the 4th term to the remaining time where the water is in the form of vapor.

Here we decided to consider meteorological data in Paris to assess the alteration of stained glass windows in the North of France. Thus, different parameters were considered:

- Temperature T: in Paris, between 1881 and 2000, the average temperature is around 12 °C (Météo-France data).
- Time t: the exposure time is 700 years to account for stained glass windows dating from the beginning of the 14th c.
- x_{rain}: the average annual precipitation is 617 mm between 1881 and 2000 (Météo-France data). The number of rainy days varies as a function of the threshold: ~110 days for precipitation >1 mm, 43 days for values > 5 mm and 16 days for values > 10 mm. Between 1961 and 1990, it has rained 548 h $year^{-1}$. Thus, the considered rain time can range between 6 and 30% (ratio of the rainy days >1 mm). However, as it does not rain all the day, the input value is 6%.
- D_{rain}: it depends on pH and temperature (Eq. (8)). The considered temperature is the average temperature in Paris (see above). The pH of rain generally varies between 5 and 8

with more extreme values. Moreover, pH can rapidly increase due to the interdiffusion if the runoff is low. That is why a range of pH between 5.6 and 8 was considered to calculate D_{rain}.

- r: on the same way, r can be calculated as a function of r_0 that depends on pH and temperature (Eq. (5)) and the affinity (Eq. (6)) that is not negligible if the flowrate is insufficient to renew the solution.
- x_{wet}: the Kelvin equation predicts capillary condensation in the porosity of a solid as a function of pore size. For a given pressure P, the Kelvin radius (R_K), i.e. the largest pore radius in which capillary condensation can occur, can be calculated:

$$R_K = \frac{-2\gamma \cdot V_{mol}}{R \cdot T \cdot \ln(RH)} \quad (10)$$

With γ the surface tension of ordinary water in equilibrium with pure water vapor ($73.9{\cdot}10^{-3}$ N m^{-1} at 12 °C for water), V_m the molar volume of the liquid ($18{\cdot}10^{-6}$ m^3 mol^{-1}), R the universal gas constant, T the temperature and RH the relative humidity.

At 12 °C, the Kelvin radius is 2 nm for 57% RH, 3 nm for 69% RH, 5 nm for 80% RH, 10 nm for 89% RH and 20 nm for 95% RH (Fig. 4). In Paris, the average RH is around 70%, which means that pores whose radius lower than 3 nm are saturated by liquid water. However, the RH strongly varies on daily scale. Between 2007 and 2010 (laboratory meteorological station), the RH was higher than 80% during 20% of time. It is difficult to estimate what is the fraction of time where the altered layer is sufficiently soaked by water so that the alteration occurs, but considering previous data (pore distribution, RH variations, rainfall events), we can arbitrarily fix a time fraction of 25%.

- D_{wet}: when the altered layer is wet, interdiffusion is the main mechanism due to the high surface of glass/volume of solution (S/V) ratio and to the low renewal of the solution and dissolution is assumed to be negligible because of high expected Si concentration. Therefore, D_{wet} can be calculated as a function of T and pH (Eq. (8)). Due to interdiffusion, pH is assumed to increase until 8 or 9.
- x_{vapor}: this parameter is the remaining time fraction after deduction of x_{rain} and x_{wet}.
- D_{vapor}: kinetic laws have still to be completed to precisely determine the diffusion coefficient. Moreover, previous experiments[91] have shown that the relation between diffusion coefficient and RH was not linear. Therefore, for this parameter, we considered values from short-term exposure, laboratory and isotope tracing experiments. Table 5 shows that all the calculated diffusion coefficients are in the order of 10^{-20} m^2 s^{-1}. Sessegolo et al.[91] have also measured a value of $1{\cdot}10^{-20}$ m^2 s^{-1} for a model glass (SG3) altered at 20 °C for 9 months. Last, Sessegolo et al.[86], thanks to D isotope tracing used to alter ancient stained glass windows, have measured diffusion coefficients of $3.6{\cdot}10^{-20}$ m^2 s^{-1} at 20 °C and 70% RH and of $4.9{\cdot}10^{-20}$ m^2 s^{-1} at 90% RH. Therefore, a value of $3.6{\cdot}10^{-20}$ m^2 s^{-1} was considered in the calculations.

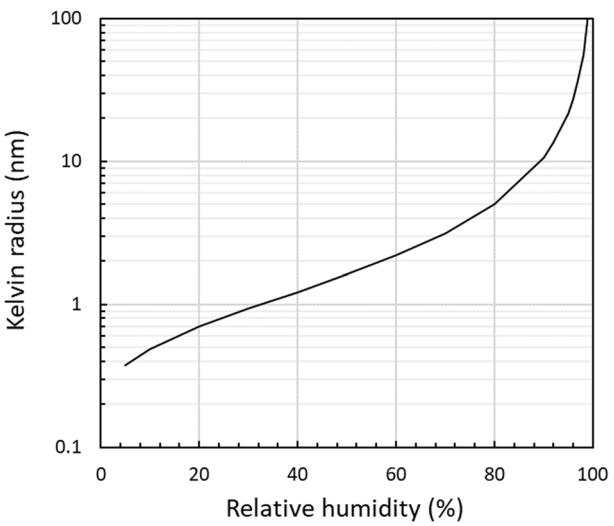

Fig. 4 Kelvin radius (in nm) as a function of relative humidity (in %). The Kelvin radius is the pore radius at which the capillary condensation would occur for a given relative humidity predicted by Kelvin equation (Eq. (10)).

The calculation of the dissolved glass or altered glass thickness (the second term in Eq. (9)) considering the initial dissolution rate (Eq. (5)) shows that, whatever the values of rain pH, the loss of material caused by dissolution is very high and not realistic (as a significant part of the glass would be lost over centuries, whereas on some ancient samples, the original surface when grisaille is present is still visible). For example, after 700 years, the dissolved thickness is around 780 µm for a rain pH of 5.6. Several hypotheses can explain that in reality the dissolved fraction is much lower. The runoff caused by rain can be insufficient to leach the glass surface or to dissolve the alteration layer. Moreover, this is not a diluted medium: the high S/V imposes to take into account the Si chemistry affinity term decreasing the dissolution rate. Moreover, the presence of an altered layer limits the direct contact of the rain with the pristine glass. This is consistent with experiments of ancient stained glass exposed to a drizzle at the laboratory[87]. At the end of the experiments, the altered layer is still present and the alteration has occurred by interdiffusion at the pristine/altered glass interface. Therefore, the second term is not considered in the following calculations and loss of material is assumed to occur by detachment of scales when the altered layer is too thick. Equation (9) becomes:

$$\mathrm{ALT} = 2\sqrt{\frac{D_{rain} \cdot x_{rain} \cdot t}{\pi}} + 2\sqrt{\frac{D_{wet} \cdot x_{wet} \cdot t}{\pi}} + 2\sqrt{\frac{D_{vapor} \cdot x_{vapor} \cdot t}{\pi}} \quad (11)$$

By considering pH_{rain} between 5.6 and 8 and pH_{wet} between 8 and 9, the predicted range of altered thickness is 138–204 µm after 700 years of alteration.

As for the exposures in real conditions, according to Gentaz[125], the total alteration thickness of the model glass subjected to precipitation is 13.8 µm on average after 3 years (between 0.6 and 25.7 µm due to numerous scale losses), while that of the sample in sheltered condition is 1.2 µm. The contact with liquid water is thus responsible for at least 12.6 µm. For the same parameters, Eq. (11) predicts after 3 years a range of 9.0 to 13.4 µm in unsheltered conditions and 2.1 µm in sheltered conditions. All the estimated results are very consistent with the observation of ancient samples and short-term samples exposed to the real atmosphere.

Moreover, Eq. (11) applied for a time of 700 years give calculated altered glass thickness of 44 to 88 µm induced by rain 6% of time (according to rain pH, 8 or 5.6), of 67 to 90 µm induced by imbibition 25% of time (according to the pH in the altered layer, 8 or 9) and 26 µm induced by the water vapor. This highlights that the alteration caused by vapor and imbibition is not negligible. These results are also in very good agreement with alteration layer thickness values measured on ancient stained glass samples (between 0 and 300 µm, see section "Alteration thickness").

Even if the effect of pollution needs to be more finely studied in terms of mechanisms and quantified in terms of kinetics, a rough sensitivity test can be conducted. High levels of pollution are expected to acidify rain or of water film, which can increase the diffusion coefficients of rainfall events (D_{rain}) and wet situation (D_{wet}). Gases (such as SO_2) can also induce secondary phases

formation (such as syngenite or gypsum) and increase the alteration rate[147]. Marine aerosols can also increase the hygroscopicity of the glass surface and open the glass structure, which favors the alteration[161]. If rain pH is 4, the altered glass thickness caused by rain can reach 139 µm. If pH of water that soaks the alteration layer decreases to 7, the altered glass thickness would increase to 120 µm. Last, if the diffusion coefficient in vapor phase is multiplied by 10 (based on short-term exposure in real conditions[29,158]), the altered glass thickness is 84 µm. The total altered glass thickness is thus 343 µm. Therefore, during the highest polluted periods (especially during the nineteenth and twentieth centuries[162]), the alteration rate has certainly increased. If these extreme conditions are considered for 200 years (over 700 years), the maximum alteration layer is 254 µm.

There is therefore a good agreement between these calculations and the observations of ancient samples. This could be surprising as this model is a mathematical simplification based on an unrealistic separation of the different environmental situations and as it is based on different assumptions that can be discussed. First, the total altered glass thickness does not result from the independent growth of three alteration layers. Beyond the mathematical formalism, these interactions should be better studied with realistic experiments (alternation of rain events and unsaturated phases) to estimate the sequential retention in the alteration layer and release of elements during the rainfall washout. Then, the role of dissolution was neglected for the benefit of the diffusion. Some short-term exposures have shown the loss of scales[37], whereas the loss of mass is relatively rare on ancient stained glass windows. On the same way, experiments in vapor phase have shown that the diffusion coefficient can change in the first months[91,150]. These issues raise the question of the representativeness of short-term experiments. However, the determination of diffusion coefficients on ancient stained glass windows using isotopic tracers[86] lifts partly this reservation. Last, average values were considered, whereas D does not evolve linearly with RH or can change with polluted atmospheres[91,158]. In parallel, uncertainties on the environmental parameters have to be reduced and their variations have to be implemented (as kinetic laws are non-linear). However, even if this model has to be improved, it has the merit of highlighting that diffusion mechanisms seem to be predominant to account for the long-term alteration.

With this in mind, Eq. (11) could be improved. Geochemical modeling could be used to precisely assess the pH at the glass surface (as a function of the rain water flow) and inside the pore network (where pH results from alteration and transport within the altered layer). Also, the speciation of Si in the altered layer could be considered to assess the intensity of the dissolution.

Besides, altered layer thickness can be variable even for one sample and many local factors can also be influent, such as local defects, microorganisms, etc. However, as a first approximation it gives good results to explain the long-term alteration over centuries. It also could allow the variations caused by temperature, RH or rain pH and rain quantity to be calculated and potentially the evolution of stained glass windows in the future in the context of climate change to be projected.

In practical terms, as the installation of protective glazing protects the outer side of the stained glass windows from direct rainfall and from wind and allows reducing both the pollutant concentration and the relative humidity levels[12,13], the alteration rate is expected to significantly decrease[11].

CONCLUSIONS AND OUTLOOK

From the literature on stained glass windows alteration, a scenario of their alteration was proposed to explain pits, cracks, laminated altered layer formation over centuries in atmospheric medium. The variability of this constantly changing environment makes the prediction over several centuries difficult. However, simple calculations based on laboratory or short-term exposures and extrapolated to long-term give good results to explain the observed apparent alteration rates of medieval stained glass windows. The results also give the respective contribution of rain, wet and dry phases on the alteration. This current modeling has of course to be improved in the future. This model could also be used to calculate the quantity of secondary phases by considering the release of the modifier ions (K^+, Ca^{2+}) that could react with atmospheric gases in specific conditions (rain pH, evaporation cycles). The studies on stained glass windows should also focus on the influence of glass composition (and structure) on the alteration and on the understanding and quantification of the role of pollutants and microorganisms.

DATA AVAILABILITY

Most of the analyzed data are compiled from the literature. New data generated during this study are included in this article.

Received: 23 December 2022; Accepted: 24 May 2023;
Published online: 17 June 2023

REFERENCES

1. Calas, G., Galoisy, L. & Cormier, L. The color of glass. In *Encyclopedia of Glass Science, Technology, History, and Culture* (eds Richet, P., Conradt, R., Takada, A. & Dyon, J.) 677–691 (John Wiley & Sons Ltd., 2021).
2. Capobianco, N. et al. The representation of skin colour in medieval stained glasses: the role of manganese. *J. Archaeol. Sci. Rep.* **38**, 103082 (2021).
3. Capobianco, N. et al. The Grande Rose of the Reims Cathedral: an eight-century perspective on the colour management of medieval stained glass. *Sci. Rep.* **9**, 3287 (2019).
4. Galoisy, L. Structure-property relationships in industrial and natural glasses. *Elements* **2**, 293–297 (2006).
5. Hunault, M. O. J. Y. et al. Thirteenth-century stained glass windows of the Sainte-Chapelle in Paris: an insight into medieval glazing work practices. *J. Archaeol. Sci. Rep.* **35**, 102753 (2021).
6. Rossano, S. et al. Glass colourations caused by Mn-Fe redox pair: application to ancient glass technology. *J. Non-Cryst. Solids* **594**, 121710 (2022).
7. Lautier, C. Les débuts du jaune d'argent dans l'art du vitrail ou le jaune d'argent à la manière d'Antoine de Pise. *Bull. Monum.* **158**, 89–107 (2000).
8. Pallot-Frossard, I. *Manuel de conservation, restauration et création de vitraux* (Ministère de la Culture et de la Communication, 2007).
9. Camuffo, D., Pagan, E., Bernardi, A. & Becherini, F. The impact of heating, lighting and people in re-using historical buildings: a case study. *J. Cult. Herit.* **5**, 409–416 (2004).
10. Maingi, E. M. et al. Historical stained-glass window laser preservation: the heat accumulation challenge. *Bol. Soc. Esp. Ceram. Vidr.* **61**, S69–S82 (2022).
11. Bernardi, A. et al. Conservation of stained glass windows with protective glazing: main results from the European VIDRIO research programme. *J. Cult. Herit.* **14**, 527–536 (2013).
12. Bernardi, A., Becherini, F., Bassato, G. & Bellio, M. Condensation on ancient stained glass windows and efficiency of protective glazing systems: two French case studies, Sainte-Chapelle (Paris) and Saint-Urbain Basilica (Troyes). *J. Cult. Herit.* **7**, 71–78 (2006).
13. Godoi, R. H. M., Kontozova, V. & Van Grieken, R. The shielding effect of the protective glazing of historical stained glass windows from an atmospheric chemistry perspective: case study Sainte Chapelle, Paris. *Atmos. Environ.* **40**, 1255–1265 (2006).
14. Gin, S. et al. An international initiative on long-term behavior of high-level nuclear waste glass. *Mater. Today* **16**, 243–248 (2013).
15. Vienna, J. D., Ryan, J. V., Gin, S. & Inagaki, Y. Current understanding and remaining challenges in modeling long-term degradation of borosilicate nuclear waste glasses. *Int. J. Appl. Glass Sci.* **4**, 283–294 (2013).
16. Prause, S. et al. Alteration of basaltic glass within the Surtsey hydrothermal system, Iceland—implication to oceanic crust seawater interaction. *J. Volcanol. Geotherm. Res.* **429**, 107581 (2022).
17. Kurkjian, C. R. & Prindle, W. R. Perspectives on the history of glass composition. *J. Am. Ceram. Soc.* **81**, 795–813 (1998).
18. Schalm, O., Janssens, K., Wouters, H. & Caluwé, D. Composition of 12–18th century window glass in Belgium: non-figurative windows in secular buildings

and stained-glass windows in religious buildings. *Spectrochim. Acta B* **62**, 663–668 (2007).
19. Barrera, J. & Velde, B. D. A study of french medieval glass composition. *Archeol. Mediev.* **19**, 81–130 (1989).
20. Wedepohl, K. H. & Simon, K. The chemical composition of medieval wood ash glass from Central Europe. *Geochemistry* **70**, 89–97 (2010).
21. Gliozzo, E. The composition of colourless glass: a review. *Archaeol. Anthropol. Sci.* **9**, 455–483 (2017).
22. Majérus, O. et al. Glass alteration in atmospheric conditions: crossing perspectives from cultural heritage, glass industry, and nuclear waste management. *NPJ Mater. Degrad.* **4**, 1–16 (2020).
23. Adlington, L. W. et al. Regional patterns in medieval European glass composition as a provenancing tool. *J. Archaeol. Sci.* **110**, 104991 (2019).
24. Sterpenich, J. & Libourel, G. Using stained glass windows to understand the durability of toxic waste matrices. *Chem. Geol.* **174**, 181–193 (2001).
25. Ferrand, J. et al. Browning phenomenon of medieval stained glass windows. *Anal. Chem.* **87**, 3662–3669 (2015).
26. Casellato, U. et al. Medieval and renaissance glass technology in Valdelsa (Florence). Part 1: raw materials, sands and non-vitreous finds. *J. Cult. Herit.* **4**, 337–353 (2003).
27. Bianchin, S. et al. Medieval and renaissance glass technology in Valdelsa (Florence). Part 2: vitreous finds and sands. *J. Cult. Herit.* **6**, 39–54 (2005).
28. Hunault, M. O. J. Y. et al. The rose of the Sainte-Chapelle in Paris: sophisticated stained glasses for late medieval painters. *C. R. Geosci.* **354**, 101–120 (2022).
29. Melcher, M. & Schreiner, M. Leaching studies on naturally weathered potash-lime–silica glasses. *J. Non-Cryst. Solids* **352**, 368–379 (2006).
30. Melcher, M. & Schreiner, M. Evaluation procedure for leaching studies on naturally weathered potash-lime-silica glasses with medieval composition by scanning electron microscopy. *J. Non-Cryst. Solids* **351**, 1210–1225 (2005).
31. Woisetschläger, G., Dutz, M., Paul, S. & Schreiner, M. Weathering phenomena on naturally weathered potash-lime-silica-glass with medieval composition studied by secondary electron microscopy and energy dispersive microanalysis. *Microchim. Acta* **135**, 121–130 (2000).
32. Silvestri, A., Molin, G. & Pomero, V. The stained glass window of the southern transept of St. Anthony's Basilica (Padova, Italy): study of glasses and grisaille paint layers. *Spectrochim. Acta B* **66**, 81–87 (2011).
33. Vilarigues, M., Fernandes, P., Alves, L. C. & da Silva, R. C. Stained glasses under the nuclear microprobe: a window into history. *Nucl. Instrum. Methods Phys. Res. B* **267**, 2260–2264 (2009).
34. Drewello, R. & Weissmann, R. Microbially influenced corrosion of glass. *Appl. Microbiol. Biotechnol.* **47**, 337–346 (1997).
35. Müller, E., Drewello, U., Drewello, R., Weißmann, R. & Wuertz, S. In situ analysis of biofilms on historic window glass using confocal laser scanning microscopy. *J. Cult. Herit.* **2**, 31–42 (2001).
36. Sessegolo, L., Verney-Carron, A., Ausset, P., Saheb, M. & Chabas, A. Effect of surface roughness on medieval-type glass alteration in aqueous medium. *J. Non-Cryst. Solids* **505**, 260–271 (2019).
37. Gentaz, L. et al. Role of secondary phases in the scaling of stained glass windows exposed to rain. *Corros. Sci.* **109**, 206–216 (2016).
38. Carmona, N. et al. Biodeterioration of historic stained glasses from the Cartuja de Miraflores (Spain). *Int. Biodeterior. Biodegrad.* **58**, 155–161 (2006a).
39. Lombardo, T. et al. Long term assessment of atmospheric decay of stained glass windows. *Corros. Eng. Sci. Technol.* **45**, 420–424 (2010).
40. Cox, G. A. & Ford, R. A. The corrosion of glass on the sea bed. *J. Mater. Sci.* **24**, 3146–3153 (1989).
41. Dal Bianco, B., Bertoncello, R., Milanese, L. & Barison, S. Glass corrosion across the alps: a surface study of chemical corrosion of glasses found in marine and ground environments. *Archaeometry* **47**, 351–360 (2005).
42. Longinelli, A., Silvestri, A., Molin, G. & Salviulo, G. 1.8 ka old glass from the Roman ship Julia Felix: glass–water oxygen isotope exchange. *Chem. Geol.* **211**, 335–342 (2004).
43. Brill, R. H. & Hood, H. P. A new method for dating ancient glass. *Nature* **189**, 12–14 (1961).
44. Cox, G. A. & Ford, B. A. The long-term corrosion of glass by ground-water. *J. Mater. Sci.* **28**, 5637–5647 (1993).
45. Doménech-Carbó, M.-T., Doménech-Carbó, A., Osete-Cortina, L. & Saurí-Peris, M.-C. A study on corrosion processes of archaeological glass from the Valencian Region (Spain) and its consolidation treatment. *Microchim. Acta* **154**, 123–142 (2006).
46. Genga, A. et al. Characterization of surface layers formed under natural environmental conditions on medieval glass from Siponto (Southern Italy). *Mater. Chem. Phys.* **111**, 480–485 (2008).
47. Gulmini, M., Pace, M., Ivaldi, G., Ponzi, M. N. & Mirti, P. Morphological and chemical characterization of weathering products on buried Sasanian glass from central Iraq. *J. Non-Cryst. Solids* **355**, 1613–1621 (2009).
48. Hasdemir, I., Striepe, S., Deubener, J. & Schmidt, B. C. Micromechanical properties of banded alterations of archaeological glass fragments. *J. Non-Cryst. Solids* **376**, 126–132 (2013).
49. Macquet, C. & Thomassin, J. H. Archaeological glasses as modelling of the behavior of buried nuclear waste glass. *Appl. Clay Sci.* **7**, 17–31 (1992).
50. Procházka, R. et al. A comparison of natural and experimental long-term corrosion of uranium-colored glass. *J. Non-Cryst. Solids* **355**, 2134–2142 (2009).
51. Römich, H. Studies of ancient glass and their application to nuclear-waste management. *MRS Bull.* **28**, 500–504 (2003).
52. Salviulo, G., Silvestri, A., Molin, G. & Bertoncello, R. An archaeometric study of the bulk and surface weathering characteristics of early Medieval (5th–7th century) glass from the Po valley, northern Italy. *J. Archaeol. Sci.* **31**, 295–306 (2004).
53. Schalm, O. & Anaf, W. Laminated altered layers in historical glass: density variations of silica nanoparticle random packings as explanation for the observed lamellae. *J. Non-Cryst. Solids* **442**, 1–16 (2016).
54. Silvestri, A., Molin, G. & Salviulo, G. Archaeological glass alteration products in marine and land-based environments: morphological, chemical and microtextural characterization. *J. Non-Cryst. Solids* **351**, 1338–1349 (2005).
55. Sterpenich, J. & Libourel, G. Water diffusion in silicate glasses under natural weathering conditions: evidence from buried medieval stained glasses. *J. Non-Cryst. Solids* **352**, 5446–5451 (2006).
56. Stroncik, N. A. & Schmincke, H.-U. Palagonite—a review. *Int. J. Earth Sci.* **91**, 680–697 (2002).
57. Dohmen, L. et al. Pattern formation in silicate glass corrosion zones. *Int. J. Appl. Glass Sci.* **4**, 357–370 (2013).
58. Kontozova-Deutsch, V., Deutsch, F., Godoi, R., Van Grieken, R. & De Wael, K. Urban air pollutants and their micro effects on medieval stained glass windows. *Microchem. J.* **99**, 508–513 (2011).
59. Bacci, M., Corallini, A., Orlando, A., Picollo, M. & Radicati, B. The ancient stained windows by Nicolò di Pietro Gerini in Florence. A novel diagnostic tool for non-invasive in situ diagnosis. *J. Cult. Herit.* **8**, 235–241 (2007).
60. Vilarigues, M. et al. Corrosion of 15th and early 16th century stained glass from the monastery of Batalha studied with external ion beam. *Mater. Charact.* **62**, 211–217 (2011).
61. Müller, W. Altérations des vitraux du Moyen-Âge. In *Programme Franco-Allemand de recherche pour la conservation des monuments historiques: colloque final* (eds Pallot-Frossard, I. & Philippon, J.) 312–329 (Exé Productions, 1999).
62. Ferrand, J. *Le phénomène de brunissement des vitraux médiévaux: critères d'identification et nature de la phase d'altération* (Université Paris-Est, 2013).
63. Barbey, P., Sterpenich, J. & Libourel, G. Altération des vitraux: produits d'altération, états d'oxydation du manganèse, effets des traitements de surface. Stained glass weathering: corrosion products, manganese oxydation states, effects of retreatments of the surface. In *Conservation commune d'un patrimoine commun* (ed. Filtz, J. F.) 61–72 (Programme franco-allemand de recherche pour la conservation des monuments historiques, 1997).
64. Schalm, O. et al. Manganese staining of archaeological glass: the characterization of Mn-rich inclusions in leached layers and a hypothesis of its formation. *Archaeometry* **53**, 103–122 (2011).
65. Sterpenich, J. *Altération des vitraux médiévaux: contribution à l'étude du comportement à long terme des verres de confinement* (Université de Nancy 1, 1998).
66. Krawczyk-Bärsch, E., Däbritz, S. & Hauffe, W. The darkening of medieval glass by oxidation of manganese. In *Conservation commune d'un patrimoine commun* (ed. Filtz, J.F.) 73–80 (Programme franco-allemand de recherche pour la conservation des monuments historiques, 1997).
67. Gin, S., Delaye, J.-M., Angeli, F. & Schuller, S. Aqueous alteration of silicate glass: state of knowledge and perspectives. *NPJ Mater. Degrad.* **5**, 1–20 (2021).
68. Doremus, R. Interdiffusion of hydrogen and alkali ions in a glass surface. *J. Non-Cryst. Solids* **19**, 137–144 (1975).
69. Ferrand, K., Abdelouas, A. & Grambow, B. Water diffusion in the simulated French nuclear waste glass SON 68 contacting silica rich solutions: experimental and modeling. *J. Nucl. Mater.* **355**, 54–67 (2006).
70. Rébiscoul, D. et al. Water penetration mechanisms in nuclear glasses by X-ray and neutron reflectometry. *J. Non-Cryst. Solids* **353**, 2221–2230 (2007).
71. Smets, B. & Lommen, T. The role of molecular water in the leaching of glass. *Phys. Chem. Glasses* **24**, 35–36 (1983).
72. Bunker, B. C. Molecular mechanisms for corrosion of silica and silicate glasses. *J. Non-Cryst. Solids* **179**, 300–308 (1994).
73. Bouyer, F., Geneste, G., Ispas, S., Kob, W. & Ganster, P. Water solubility in calcium aluminosilicate glasses investigated by first principles techniques. *J. Solid State Chem.* **183**, 2786–2796 (2010).
74. Geneste, G., Bouyer, F. & Gin, S. Hydrogen–sodium interdiffusion in borosilicate glasses investigated from first principles. *J. Non-Cryst. Solids* **352**, 3147–3152 (2006).
75. White, A. F. & Claassen, H. C. Kinetic model for the short-term dissolution of a rhyolitic glass. *Chem. Geol.* **28**, 91–109 (1980).

76. Houser, C. A., Herman, J. S., Tsong, I. S. T., White, W. B. & Lanford, W. A. Sodium-hydrogen interdiffusion in sodium silicate glasses. *J. Non-Cryst. Solids* **41**, 89–98 (1980).
77. Lanford, W. A. et al. Hydration of soda-lime glass. *J. Non-Cryst. Solids* **33**, 249–266 (1979).
78. Tsong, I. S. T. et al. Evidence for interdiffusion of hydronium and alkali ions in leached glasses. *Appl. Phys. Lett.* **39**, 669–670 (1981).
79. Dran, J.-C., Petit, J.-C., Trotignon, L., Paccagnella, A. & Mea, G. D. Hydration mechanisms of silicate glasses: discussion of the respective role of ion exchange and water permeation. In *MRS Online Proceedings Library Archive* 127 (1988).
80. Hellmann, R. et al. Nanometre-scale evidence for interfacial dissolution-reprecipitation control of silicate glass corrosion. *Nat. Mater.* **14**, 307–311 (2015).
81. Lenting, C. et al. Towards a unifying mechanistic model for silicate glass corrosion. *NPJ Mater. Degrad.* **2**, 1–10 (2018).
82. Ma, T. et al. A mechanistic model for long-term nuclear waste glass dissolution integrating chemical affinity and interfacial diffusion barrier. *J. Nucl. Mater.* **486**, 70–85 (2017).
83. Valle, N. et al. Elemental and isotopic (29Si and 18O) tracing of glass alteration mechanisms. *Geochim. Cosmochim. Acta* **74**, 3412–3431 (2010).
84. Leissner, J. The effect of air pollution on glass. In *The Effects of Air Pollution on the Built Environment* (ed. Brimblecombe, P.) 249–265 (World Scientific, 2003).
85. Sessegolo, L. *Utilisation de traceurs isotopiques pour l'étude des mécanismes et des cinétiques d'altération des verres de vitraux en milieu atmosphérique* (Université Paris-Est, 2018).
86. Sessegolo, L. et al. Long-term weathering rate of stained-glass windows using H and O isotopes. *NPJ Mater. Degrad.* **2**, 1–9 (2018).
87. Verney-Carron, A., Saheb, M., Loisel, C., Duhamel, R. & Remusat, L. Use of hydrogen isotopes to understand stained glass weathering. *Procedia Earth Planet. Sci.* **13**, 64–67 (2015).
88. Verney-Carron, A. et al. Understanding the mechanisms of Si–K–Ca glass alteration using silicon isotopes. *Geochim. Cosmochim. Acta* **203**, 404–421 (2017).
89. Asay, D. B. & Kim, S. H. Evolution of the adsorbed water layer structure on silicon oxide at room temperature. *J. Phys. Chem. B* **109**, 16760–16763 (2005).
90. Ebert, W. L., Hoburg, R. F. & Bates, J. K. The sorption of water on obsidian and a nuclear waste glass. *Phys. chem. Glasses* **32**, 133–137 (1991).
91. Sessegolo, L. et al. Alteration of potash-lime silicate glass in atmospheric medium: study of mechanisms and kinetics using 18O and D isotopes. *J. Non-Cryst. Solids* **570**, 121020 (2021).
92. Anovitz, L. M., Cole, D. R. & Fayek, M. Mechanisms of rhyolitic glass hydration below the glass transition. *Am. Mineral.* **93**, 1166–1178 (2008).
93. Kudriavtsev, Y. U., Asomoza-Palacio, R. & Manzanilla-Naim, L. Interaction of water vapor with silicate glass surfaces: mass-spectrometric investigations. *Tech. Phys. Lett.* **43**, 447–449 (2017).
94. Alloteau, F. et al. New insight into atmospheric alteration of alkali-lime silicate glasses. *Corros. Sci.* **122**, 12–25 (2017).
95. Kudriavtsev, Y., Avendano, M., Ramirez, G., Asomoza-Palacio, R. & Manzanilla-Naim, L. Water vapor interaction with borosilicate glass. *Solid State Ion.* **321**, 122–125 (2018).
96. Cummings, K., Lanford, W. A. & Feldmann, M. Weathering of glass in moist and polluted air. *Nucl. Instrum. Methods Phys. Res. B* **136–138**, 858–862 (1998).
97. Fearn, S., McPhail, D. S., Morris, R. J. H. & Dowsett, M. G. Sodium and hydrogen analysis of room temperature glass corrosion using low energy Cs SIMS. *Appl. Surf. Sci.* **252**, 7070–7073 (2006).
98. Gentaz, L., Lombardo, T., Chabas, A., Loisel, C. & Verney-Carron, A. Impact of neocrystallisations on the SiO2–K2O–CaO glass degradation due to atmospheric dry depositions. *Atmos. Environ.* **55**, 459–466 (2012).
99. Wexler, A. S. & Seinfeld, J. H. Second-generation inorganic aerosol model. *Atmos. Environ.* **25**, 2731–2748 (1991).
100. Palomar, T., Chabas, A., Bastidas, D. M., de la Fuente, D. & Verney-Carron, A. Effect of marine aerosols on the alteration of silicate glasses. *J. Non-Cryst. Solids* **471**, 328–337 (2017).
101. Palomar, T. Chemical composition and alteration processes of glasses from the Cathedral of León (Spain). *Bol. Soc. Esp. Ceram. Vidr.* **57**, 101–111 (2018).
102. Lombardo, T. et al. Characterisation of complex alteration layers in medieval glasses. *Corros. Sci.* **72**, 10–19 (2013).
103. Krumbein, W. E., Urzì, C. E. & Gehrmann, C. Biocorrosion and biodeterioration of antique and medieval glass. *Geomicrobiol. J.* **9**, 139–160 (1991).
104. Tennent, N. H. Fungal growth on medieval stained glass. *J. Br. Soc. Master Glass Painters* **17**, 64–68 (1981).
105. Rodrigues, A. et al. Fungal biodeterioration of stained-glass windows. *Int. Biodeterior. Biodegrad.* **90**, 152–160 (2014).
106. Piñar, G. et al. Microscopic, chemical, and molecular-biological investigation of the decayed medieval stained window glasses of two Catalonian churches. *Int. Biodeterior. Biodegrad.* **84**, 388–400 (2013).
107. Corrêa Pinto, A. M. et al. Fungal biodeterioration of stained-glass windows in monuments from Belém do Pará (Brazil). *Int. Biodeterior. Biodegrad.* **138**, 106–113 (2019).
108. Marvasi, M. et al. Bacterial community analysis on the Mediaeval stained glass window "Natività" in the Florence Cathedral. *J. Cult. Herit.* **10**, 124–133 (2009).
109. Valbi, V. et al. Bacterial diversity on stained glass windows. *Int. Biodeterior. Biodegrad.* **177**, 105529 (2023).
110. Perez y Jorba, M., Dallas, J. P., Bauer, C., Bahezre, C. & Martin, J. C. Deterioration of stained glass by atmospheric corrosion and micro-organisms. *J. Mater. Sci.* **15**, 1640–1647 (1980).
111. Anaf, W. Study on the formation of heterogeneous structures in leached layers during the corrosion process of glass. *CeROArt* **1561** https://doi.org/10.4000/ceroart.1561 (2010).
112. Messiga, B. & Riccardi, M. P. Alteration behaviour of glass panes from the medieval Pavia Charterhouse (Italy). *J. Cult. Herit.* **7**, 334–338 (2006).
113. Valbi, V. et al. Impact of biogenic exudates on the dissolution and browning of stained glass windows. *Int. Biodeterior. Biodegrad.* **173**, 105442 (2022).
114. Valbi, V., Perez, A., Verney-Carron, A. & Rossano, S. Impact of a Mn-oxidizing bacterial strain on the dissolution and browning of a Mn-bearing potash-lime silicate glass. *NPJ Mater. Degrad.* **7**, 1–13 (2023).
115. Gorbushina, A. A. & Palinska, K. A. Biodeteriorative processes on glass: experimental proof of the role of fungi and cyanobacteria. *Aerobiologia* **15**, 183–192 (1999).
116. Desmau, M. et al. How microbial biofilms control the environmental fate of engineered nanoparticles? *Front. Environ. Sci.* **8**, 82 (2020).
117. Orial, G., Warscheid, T., Bousta, F. & Loisel, C. Incidence bactérienne dans le phénomène de brunissement des vitraux anciens. *Actual Chim.* **312–313**, 34–39 (2007).
118. Nuyts, G. et al. Study of the early stages of Mn intrusion in corroded glass by means of combined SR FTIR/μXRF imaging and XANES spectroscopy. *Procedia Chem.* **8**, 239–247 (2013).
119. Valbi, V. *Brunissement des vitraux médiévaux: approche biogéochimique pour la compréhension d'un phénomène d'altération complexe* (Université Paris-Est, 2020).
120. Watkinson, D., Weber, L. & Anheuser, K. Staining of archaeological glass from manganese-Rich environments. *Archaeometry* **47**, 69–82 (2005).
121. Newton, R. Recent views on ancient glasses. *Glass Technol.* **21**, 173-183 (1980).
122. Paul, A. Chemical durability of glasses; a thermodynamic approach. *J. Mater. Sci.* **12**, 2246–2268 (1977).
123. Davison, S. *Conservation and Restoration of Glass* (Elsevier Ltd., 2006).
124. Alloteau, F. et al. Evidence for different behaviors of atmospheric glass alteration as a function of glass composition. *NPJ Mater. Degrad.* **4**, 1–11 (2020).
125. Gentaz, L. *Simulation et modélisation de l'altération des verres de composition médiévale dans l'atmosphère urbaine*. (Université Paris-Est, 2011).
126. Gentaz, L., Lombardo, T., Loisel, C., Chabas, A. & Vallotto, M. Early stage of weathering of medieval-like potash-lime model glass: evaluation of key factors. *Environ. Sci. Pollut. Res. Int.* **18**, 291–300 (2011).
127. Geotti-Bianchini, F., Nicola, C., Preo, M., Vallotto, M. & Verita, M. MicroIRRS and EPMA study of the weathering of potash-lime-silicate glasses. *Riv. Stn. Sper. Vetro* **35**, 49–61 (2005).
128. Munier, I., Lefèvre, R., Geotti-Bianchini, F. & Verità, M. Influence of polluted urban atmosphere on the weathering of low durability glasses. *Glass Technol.* **43**, 225–237 (2002).
129. Tidblad, J. et al. Effects of air pollution on materials and cultural heritage: ICP materials celebrates 25 years of research. *Int. J. Corros.* **2012**, e496321 (2012).
130. Boksay, Z., Bouquet, G. & Dobos, S. The kinetics of the formation of leached layers on glass surfaces. *Phys. Chem. Glasses* **9**, 69–71 (1968).
131. Römich, H. Laboratory experiments to simulate corrosion on stained glass windows. In *The Conservation of Glass and Ceramics: Research, Practice and Training* (ed. Tennent, N. H.) 57–65 (James & James, 1999).
132. Sterpenich, J. Crystal-chemistry of alteration products of vitrified wastes: implications on the retention of polluting elements. *Waste Manag.* **28**, 120–132 (2008).
133. Cooper, G. I. & Cox, G. A. The aqueous corrosion of potash-lime-silica glass in the range 10–250°C. *Appl. Geochem.* **11**, 511–521 (1996).
134. Carmona, N., García-Heras, M., Gil, C. & Villegas, M. A. Chemical degradation of glasses under simulated marine medium. *Mater. Chem. Phys.* **94**, 92–102 (2005).
135. Vilarigues, M. & da Silva, R. C. Characterization of potash-glass corrosion in aqueous solution by ion beam and IR spectroscopy. *J. Non Cryst. Solids* **352**, 5368–5375 (2006).
136. De Bardi, M., Hutter, H. & Schreiner, M. ToF-SIMS analysis for leaching studies of potash–lime–silica glass. *Appl. Surf. Sci.* **282**, 195–201 (2013).
137. Tournié, A., Ricciardi, P. & Colomban, P. H. Glass corrosion mechanisms: a multiscale analysis. *Solid State Ion.* **179**, 2142–2154 (2008).

138. De Ferri, L., Lottici, P. P. & Vezzalini, G. Characterization of alteration phases on Potash–Lime–Silica glass. *Corros. Sci.* **80**, 434–441 (2014).
139. Vilarigues, M. & da Silva, R. C. The effect of Mn, Fe and Cu ions on potash-glass corrosion. *J. Non-Cryst. Solids* **355**, 1630–1637 (2009).
140. Sessegolo, L. et al. Alteration rate of medieval potash-lime silicate glass as a function of pH and temperature: a low pH-dependent dissolution. *Chem. Geol.* **550**, 119704 (2020).
141. Advocat, T., Crovisier, J. L., Vernaz, E., Ehret, G. & Charpentier, H. Hydrolysis of R7T7 nuclear waste glass in dilute media: mechanisms and rate as a function of pH. In *MRS Online Proceedings Library Archive* 212 (1990).
142. Gislason, S. R. & Oelkers, E. H. Mechanism, rates, and consequences of basaltic glass dissolution: II. An experimental study of the dissolution rates of basaltic glass as a function of pH and temperature. *Geochim. Cosmochim. Acta* **67**, 3817–3832 (2003).
143. Hamilton, J. P., Brantley, S. L., Pantano, C. G., Criscenti, L. J. & Kubicki, J. D. Dissolution of nepheline, jadeite and albite glasses: toward better models for aluminosilicate dissolution. *Geochim. Cosmochim. Acta* **65**, 3683–3702 (2001).
144. Inagaki, Y., Kikunaga, T., Idemitsu, K. & Arima, T. Initial dissolution rate of the international simple glass as a function of pH and temperature measured using microchannel flow-through test method. *Int. J. Appl. Glass Sci.* **4**, 317–327 (2013).
145. Verney-Carron, A., Gin, S., Frugier, P. & Libourel, G. Long-term modeling of alteration-transport coupling: application to a fractured Roman glass. *Geochim. Cosmochim. Acta* **74**, 2291–2315 (2010).
146. Schott, J., Pokrovsky, O. S. & Oelkers, E. H. The link between mineral dissolution/precipitation kinetics and solution chemistry. *Rev. Mineral. Geochem.* **70** 207–258 (2009).
147. Boehm, T. The influence of temperature, relative humidity and SO2 concentration on weathering of glass. in *Proceedings of the 5th ESG Conference* 49–55 (1999).
148. Carmona, N., Villegas, M. A. & Fernández Navarro, J. M. Corrosion behaviour of R2O–CaO–SiO2 glasses submitted to accelerated weathering. *J. Am. Ceram. Soc.* **25**, 903–910 (2005).
149. Melcher, M., Schreiner, M. & Kreislova, K. Artificial weathering of model glasses with medieval compositions—an empirical study on the influence of particulates. *Phys. Chem. Glas.: Eur. J. Glass Sci. Technol. B* **49**, 346–356 (2008).
150. Alloteau, F. et al. Temperature-dependent mechanisms of the atmospheric alteration of a mixed-alkali lime silicate glass. *Corros. Sci.* **159**, 108129 (2019).
151. Bouakkaz, R. *Altération aqueuse et hydratation en phase vapeur du verre SON68 à basse température (35-90°C)*. (Ecole des Mines de Nantes, 2014).
152. Abrajano, T. A., Bates, J. K. & Mazer, J. J. Aqueous corrosion of natural and nuclear waste glasses II. Mechanisms of vapor hydration of nuclear waste glasses. *J. Non-Cryst. Solids* **108**, 269–288 (1989).
153. Bouakkaz, R., Abdelouas, A. & Grambow, B. Kinetic study and structural evolution of SON68 nuclear waste glass altered from 35 to 125 °C under unsaturated H2O and D2O18 vapour conditions. *Corros. Sci.* **134**, 1–16 (2018).
154. Moriya, Y. & Nogami, M. Hydration of silicate glass in steam atmosphere. *J. Non-Cryst. Solids* **38–39**, 667–672 (1980).
155. Neeway, J. J. *The Alteration of the SON68 Reference Waste Glass in Silica Saturated Conditions and in the Presence of Water Vapor*. (Université de Nantes, 2011).
156. Mazer, J. J., Stevenson, C. M., Ebert, W. L. & Bates, J. K. The experimental hydration of obsidian as a function of relative humidity and temperature. *Am. Antiq.* **56**, 504–513 (1991).
157. Lombardo, T. et al. Dose–response function for the soiling of silica–soda–lime glass due to dry deposition. *Sci. Total Environ.* **408**, 976–984 (2010).
158. Woisetschläger, G. & Schreiner, M. *Report No 27: Evaluation of Decay to Glass Samples after 1 and 2 Years of Exposure*. (UN/ECE International co-operative programme on effects on materials, including historic and cultural monuments, 1998).
159. Gin, S. et al. Origin and consequences of silicate glass passivation by surface layers. *Nat. Commun.* **6**, 6360 (2015a).
160. Knudsen, M. Die Gesetze der Molekularströmung und der inneren Reibungsströmung der Gase durch Röhren. *Ann. Phys.* **333**, 75–130 (1909).
161. Palomar, T., de la Fuente, D., Morcillo, M., Alvarez de Buergo, M. & Vilarigues, M. Early stages of glass alteration in the coastal atmosphere. *Build. Environ.* **147**, 305–313 (2019).
162. Brimblecombe, P. & Lefèvre, R.-A. Weathering of materials at Notre-Dame from changes in air pollution and climate in Paris, 1325–2090. *J. Cult. Herit.* **50**, 88–94 (2021).
163. Garcia-Vallès, M. & Vendrell-Saz, M. The glasses of the transept's rosette of the Cathedral of Tarragona: characterization, classification and decay. *Bol. Soc. Esp. Ceram. Vidr.* **41**, 217–224 (2002).
164. Garcia-Vallès, M., Gimeno-Torrente, D., Martínez-Manent, S. & Fernandez-Turiel, J. L. Medieval stained glass in a Mediterranean climate: typology, weathering and glass decay, and associated biomineralization processes and products. *Am. Mineral.* **88**, 1996–2006 (2003).
165. Carmona, N., García-Heras, M., Gil, C. & Villegas, M. A. Vidrios y grisallas del s. XV de la Cartuja de Miraflores (Burgos): caracterización y estado de conservación. *Bol. Soc. Esp. Ceram. Vidr.* **44**, 251–258 (2005).
166. Carmona, N., Villegas, M. A. & Navarro, J. M. F. Characterisation of an intermediate decay phenomenon of historical glasses. *J. Mater. Sci.* **41**, 2339–2346 (2006b).
167. Marchesi, V., Messiga, B. & Riccardi, M. P. Window panes of the Certosa di Pavia: chemical composition, microstructure and alteration. *Surf. Eng.* **21**, 397–401 (2005).
168. Orlando, A., Olmi, F., Vaggelli, G. & Bacci, M. Mediaeval stained glasses of Pisa Cathedral (Italy): their composition and alteration products. *Analyst* **121**, 553–558 (1996).
169. Gillies, K. J. S. & Cox, A. Decay of medieval stained glass at York, Canterbury and Carlisle. I: composition of the glass and its weathering products. *Glastechn. Ber.* **61**, 75–84 (1988).
170. Fernandes, P., Vilarigues, M., Alves, L. C. & da Silva, R. C. Stained glasses from Monastery of Batalha: non-destructive characterisation of glasses and glass paintings. *J. Cult. Herit.* **9**, 5–9 (2008).
171. Bräutigam, U., Bürger, H. & Völksch, G. Investigations into structure and composition of gel layers on medieval window glasses of the Katharinenkirche, Oppenheim (Germany), and the Cathedral St. Gatien, Tours (France). *Glass Sci. Technol. - Glastechn. Ber.* **68**, 29–33 (1995).
172. Bräutigam, U. & Bürger, H. Untersuchugen zur Struktur and Zusammensetzung von Gel-Schichten auf mittelalterlichen Kirchenfenstern der Kirchen in Oppenheim und Tours/Etude sur la composition et la structure de la couche de gel de vitraux du moyen-âge provenant d'Oppenheim et Tours. In *Conservation Commune d'un Patrimoine Commun* (ed. von Welck, S. F.) 237–244 (Programme Franco-Allemand de Recherche pour la Conservation des Monuments Historiques, 1993).
173. Perez y Jorba, M. La pollution atmosphérique et la corrosion des verres. In *Stained Glass* (ed. Sri Lanka National Committee of ICOMOS) 218–227 (International Council of Monuments and Sites, 1993).
174. Perez y Jorba, M., Mazerolles, L., Michel, D., Rommeluere, M. & Bahezre, J.-C. Etude du processus d'altération des vitraux de la cathédrale de Tours. Analyse des verres. Rôle des éléments mineurs. Etude des grisailles/Untersuchung der Verwitterungs-prozesse der Glasfenster der Kathedrale in Tours. Analyse der Glasscheiben. Rolle der Spurenelemente. Untersuchung der Verbräunung. In *Conservation Commune d'un Patrimoine Commun* (ed. von Welck, S. F.) 213–220 (Programme Franco-Allemand de Recherche pour la Conservation des Monuments Historiques, 1993).
175. Farges, F. et al. Durability of silicate glasses: an historical approach. In *AIP Conference Proceedings* vol. 882 44–50 (American Institute of Physics, 2007).
176. Schreiner, M. Deterioration of stained medieval glass by atmospheric attack. Part 1. Scanning electron microscopic investigations of the weathering phenomena. *Glastechn. Ber.* **61**, 197–204 (1988).
177. Schreiner, M. Deterioration of stained medieval glass by atmospheric attack. Part 2. Secondary ion mass spectrometry analysis of the naturally weathered glass surfaces. *Glastechn. Ber.* **61**, 223–229 (1988).
178. Falcone, R. et al. SEM-EDS, EPMA and MRS analysis of neo-crystallisations on weathered glasses. In *IOP Conf. Series: Materials Science and Engineering* 7 1–8 (2010).
179. Munier, I., Lefèvre, R. & Losno, R. Atmospheric factors influencing the formation of neocrystallisations on low durability glass exposed to urban atmosphere. *Glass Technol.* **43C**, 114–124 (2002).
180. Palomar, T., Redol, P., Cruz Almeida, I., Pereira da Silva, E. & Vilarigues, M. The influence of environment in the alteration of the stained-glass windows in Portuguese monuments. *Heritage* **1**, 365–376 (2018).

ACKNOWLEDGEMENTS

The authors would like to thank the French National Research Agency (ANR) for their financial support (GLAM project). We would like to sincerely thank the two reviewers and the associate editor for their thorough comments which helped to improve this article.

AUTHOR CONTRIBUTIONS

A.V.C. and L.S. wrote the manuscript with contributions from all the authors that have worked together for many years on the alteration of stained glass windows. C.V. performed the N_2 adsorption measurements.

COMPETING INTERESTS

The authors declare no competing interests.

ADDITIONAL INFORMATION

Supplementary information The online version contains supplementary material available at https://doi.org/10.1038/s41529-023-00367-0.

Correspondence and requests for materials should be addressed to Aurélie Verney-Carron.

Reprints and permission information is available at http://www.nature.com/reprints

Publisher's note Springer Nature remains neutral with regard to jurisdictional claims in published maps and institutional affiliations.